Department of Mechanical Engineering

Division of Mechanics

ISRN LUTFD2/TFME – 18/5040 – SE(1-79)

DETERMINATION OF THE STRESSES PRESENT IN A HY-VO CHAIN SPROCKET USING MULTIBODY SIMULATION AND FINITE ELEMENT ANALYSIS

Degree Project by

Henrik Larsson

Supervisors:
Mattias Svahn, BorgWarner Sweden
Per Hansson, Division of Mechanics
Aylin Ahadi, Division of Mechanics

Printed by Media-Tryck, Lund, Sweden

For information address:

Division of Mechanics, Lund University, Box 118, SE-211 00 Lund, Sweden

Homepage: http://www.mek.lth.se

Acknowledgments

Many thanks to BorgWarner AB Sweden for having me and providing me with the resources required for constructing this master thesis. A special appreciation to Mattias Svahn for answering all my questions and guiding me towards salvation. Also big thanks to Per Hansson and Aylin Ahdi for their assistance throughout the project.

Abstract

In this master thesis, a new way of approaching the dynamic loads on a Hy-Vo chain sprocket was investigated and analyzed. Though the approach was not new on the market, it was new to BorgWarner, whose calculations on the matter to this date have been based on approximations.

The objective for investigation is in the long end to choose optimal material properties of the sprockets to meet the requirement and to be able to virtually verify expected mechanical life. The optimization is cost-driven, with the aim to see whether or not a change in manufacturing method to powder metallurgy is possible.

The work was set to three major parts; first, the multi-body simulation, where the force levels, and force distribution between sprocket teeth, are analyzed and calculated. Second, to determine the stress levels the sprocket teeth experience, an analytical contact analysis using hertizan theory was used, and the finite element method to determine the tooth root bending stresses. Third, the fatigue calculation was done using Palmgren-Miner rule on cumulative damage.

Sammanfattning

I detta examensjobb undersöktes och analyserades ett nytt tillvägagångsätt för beräkning av de dynamiska krafterna som verkar på ett kedjekugghjul av typen Hy-Vo. Även om tillvägagångssättet inte var nytt på marknaden så var det nytt för BorgWarner, vars beräkningar tills idag har varit baserade på uppskattningar.

Målsättningen i det långa loppet handlar om att välja optimala materialegenskaper för kedjekugghjulen som uppfyller kraven samt att virtuellt kunna verifiera det förväntade mekaniska livet. Optimeringen är kostnadsdriven, med målsättningen att se huruvida ett byte av tillverkningsmetod till pulvermetallurgi är möjlig.

Arbetet var fördelat på tre huvuddelar; Först analyserades och beräknades kraftnivåerna och kraftfördelningen mellan kuggtänderna i flera flerkroppssimuleringar. Därefter bestämdes spänningsnivåerna genom en analytisk kontaktanalys genom Hertz teori, samt finita elementmetoden användes för att bestämma tandrotsspänningarna. Slutligen utfördes utmattningsberäkning via Palmgren-Miners lag om kumulativ skada.

Symbol	Unit	Description
F	N	Force
F_n	N	Normal force
F_t	N	Tangentiel force
M	Nm	Torque
ω	deg/s	Angular velocity
T	N	Chain tension
z		Number of teeth
m	mm	Module
α_t	deg	Pressure angle
D	mm	Pitch diameter
D_{tip}	mm	Top diameter
D_{bot}	mm	Root diameter
R_{tip}	mm	Top radius
R_{bot}	mm	Root radius
R_t	mm	Pitch radius / Reference radius
g	mm	Base circle radius
L	mm	Over pin measurement
r	mm	Pin diameter
Ψ	deg	Contact angle
s	mm	Tooth width
h	mm	Tooth height
b	mm	Face width
b_{link}	mm	Link width
ρ	mm	Radius of curvature
x		Addendum correction factor
h_{oa}		Rack addendum factor
h_{ot}		Rack dedendum factor
Y_f		Form factor
Y_s		Stress correction factor
Y_β		Helix factor
Y_B		Rim thickness factor
Y_{DT}		Deep tooth factor
E	GPa	Young’s modulus
E^*	GPa	Effective Young’s modulus
ν		Poisson’s ratio

Abbreviations

ISO	International Organization for Standardization
AWD	All-Wheel-Drive
FEM	Finite element method
CAD	Computer-aided design
PM	Powder metallurgy

Table of Contents

1. Background

1.1 About the company

BorgWarner PDS is a company who produces active AWD systems, such as active clutches for rear axles to transfer cases for the automotive industry with the main focus on personal cars. BorgWarner is represented in 17 different countries and has circa 29’000 employees [1] , of which 350 is located in Landskrona, Sweden.

1.2 General about BorgWarner AWD

An active AWD system allows all four wheels to be driven with the same source of power, traditionally a combustion engine. In the traditional BorgWarner AWD system where a transfer case is employed, the torque is distributed using a clutch, a chain of the type Hy-Vo and the corresponding sprockets. The Hy-Vo chain is a product from BorgWarner Morse Systems.
A high pressure pump hydraulically activates the clutch, to which the chain and sprockets are connected to, which in turns drives the wheels.. The system is computer controlled, where several parameters are taken into account, such as wheel slipping and velocity to name a few.

1.3 Background

In the D7a transfer case considered, BorgWarner AWD system is using a silent sprocket chain drive to transfer the torque from the cardan shaft to the front wheel cardan shaft. The use of silent chain is due to noise reduction, smoother torque transfer and a better load carrying capability. Unlike the more traditionally roller chain, the silent chain is composed of links which mate with the sprockets having an involute profile, making the engagement smoother. The smooth engagement reduces the so-called polygonal effect, which in effect is a excitation to the system. The excitation frequency is proportional to sprocket tooth number and rotational speed [2]. Reduction of polygonal effect will lead to lower noise, vibration and harshness, NVH

1.4 Problem description

The chain drive consists of three major parts; the chain and the two sprockets on either axis. BorgWarner Morse TEC supplies the chain, together with detailed prints on the matching sprocket geometry. The sprockets are, however, manufactured by subcontractors, and the materials they are manufactured of depend strongly on application, geometry of the complete sprocket wheel, and manufacturing location.
When designing the sprocket wheel and choosing the material, it is based upon an approximate load distribution between the teeth, see figure 1. This load distribution is as follows:

- The first tooth engaged carries forty percent of the load.
- The second tooth engages carries thirty percent of the load.
- The third tooth engaged carries twenty percent of the load.
- The fourth tooth engaged carries ten percent of the load.
- The rest of the teeth engaged carry no load.

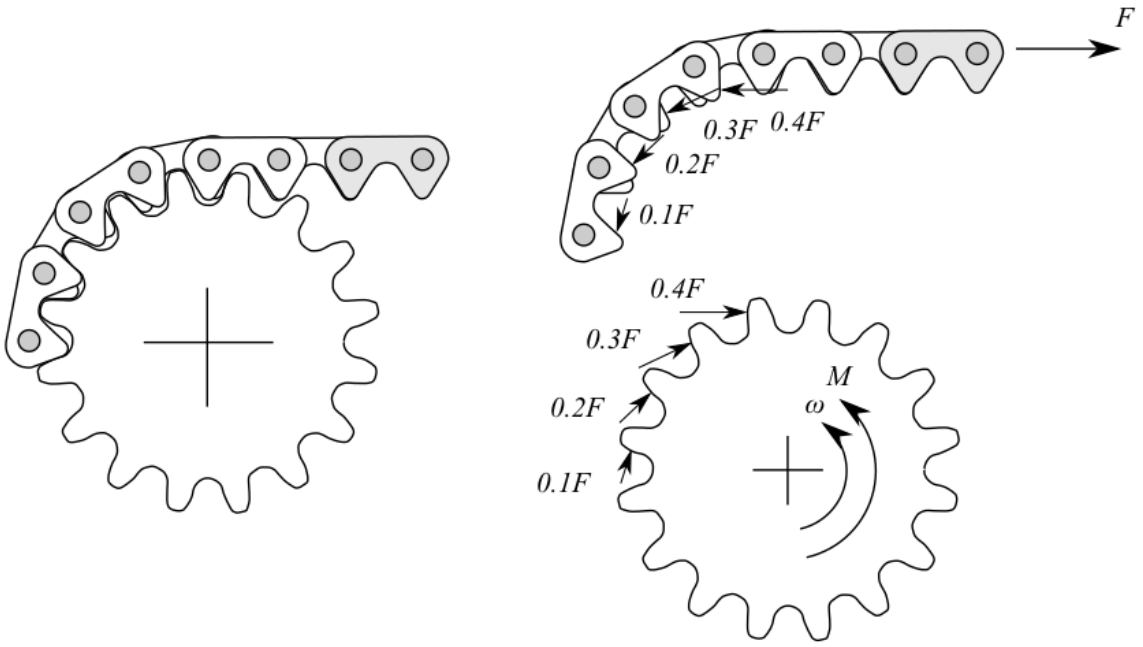

Figure 1. Load distribution between the teeth

This approximation is a rough picture of the reality, and a quite conservative such. The stresses in the sprockets are directly affected by the load distribution over the teeth. The fatigue in the sprockets is directly affected by the stresses, and thus, the performance and mechanical life of the sprocket, and in the end, the transfer case, is directly related to the load variation between the teeth.

In BorgWarner's quest of cost-optimized sprocket and chain size and sprocket material, an detailed analysis of the load distribution between the sprocket teeth is needed

1.5 Delimitations

The objective of the work carried out was set from the beginning to only focus on the sprockets and not the chain. The chain is produced and taken full responsibility for by Morse TEC and is presumably optimized in their line of development. Thus, only the sprockets are simulated and calculated upon.

1.6 Expectations

The work carried out in this thesis will hopefully improve the current design and dimensioning from a cost and production perspective. The company wishes to cost-optimize, where one path is to make the sprockets of powder metal, which requires a validation of the strength of the sprockets. Furthermore, same validation of the current product is sought after, and this thesis will substantiate these requests.

1.7 Involved persons

From BorgWarner AB Sweden, Landskrona
Mattias Svahn, Supervisor
Warren Bates, Supervisor

From Lund University, Lund
Per Hansson, Supervisor
Aylin Ahdi, Assistant supervisor
Solveig Melin, Examiner

1.8 Resources

The project is divided into three major parts; the multi-body simulation, the geometry analysis using FEM and the fatigue calculation.
The multi-body simulation will take place at LTH, where the necessary software is located. The rest of the project will take place on both LTH and BorgWarner, depending on which software in use.
LTH supplies the required software for multi-body simulation, whereas BorgWarner supplies the rest of the necessary equipment.

2. Introduction

A transfer case is a part of an AWD system which allows torque to be transmitted to all wheels. The transfer case distributes the torque and rotational speed coming from the engine via the gearbox to two outputs: the cardan shaft going to the rear axle and the cardan shaft going to the front axle, see figure 2. How this distribution is carried out varies from transfer case to transfer case, but one setup is when the cardan shaft to the rear is directly linked to the incoming shaft, and the cardan shaft to the front has variable torque transfer via a clutch. In order to transfer torque to the cardan shaft going to the front, a chain is used to connect two sprockets; one on the input (driving) shaft and one on the cardan (driven) shaft.

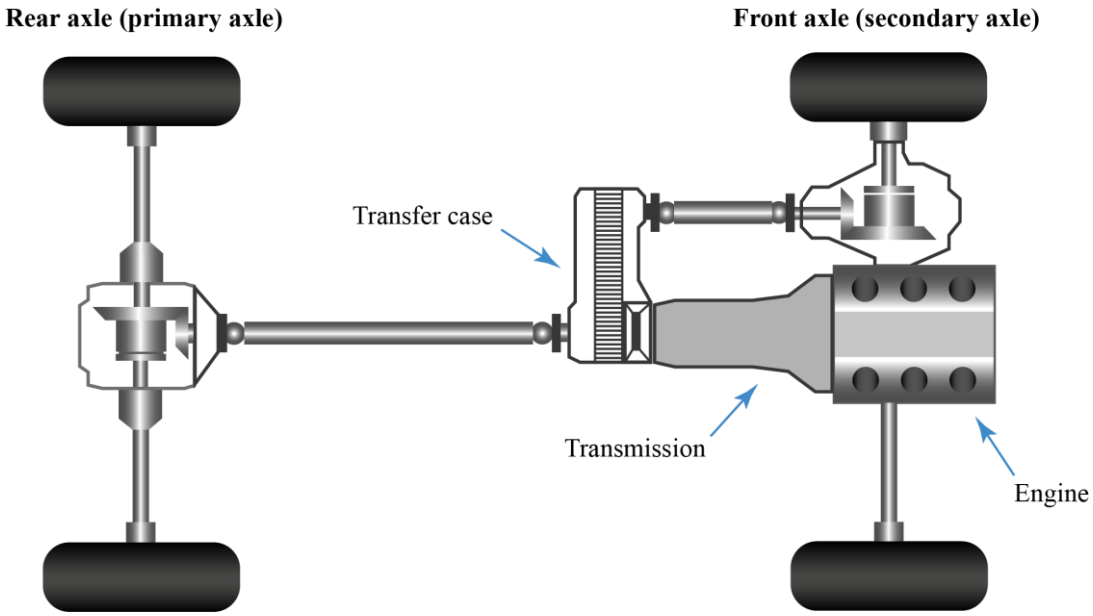

Figure 2. Transfer case placement

2.1 Transfer case drive type

In general, there are two different drive types when it comes to transfer cases; the gear-driven and the chain-driven. The gear-driven uses as the name imply a set of gears to transfer the torque. These transfer cases are typically capable of higher torque levels but are heavier and more space consuming than their chain-driven peer. The chain-driven uses a chain to transfer the torque, with lighter units as an advantage. The weight reduction is due to the chain weighs less than one extra gear wheel and two additional bearings. The shaft distance in the transfer case considered is relatively long which makes it easier to use a chain. These are the major reasons why the chain is employed in the transfer case.

In general, it is more common for the automotive industry to use chain-driven transfer cases in personal cars, compact trucks and SUVs, whereas in large trucks and heavy equipment, the gear-driven is more common.

2.2 Type of chain

The chain employed is a so-called silent chain, or inverted-tooth chain. The chain engages with the teeth with limiting sliding, and combined with the reduction of the polygonal effect, the noise inducement is limited [2]. This makes it very advantageously to use the silent chain, and is the reason why it is used.

2.3 Problems concerning the current model

The load distribution between the teeth is today done via a conservative approach. The distribution dictates the dimensioning of the sprockets, and are one of the major sources of error in expected fatigue life. The distribution is as follows;

- The first tooth engaged carries forty percent of the load.
- The second tooth engages carries thirty percent of the load.
- The third tooth engaged carries twenty percent of the load.
- The fourth tooth engaged carries ten percent of the load.
- The rest of the teeth engaged carry no load.

which can be depicted as in figure 3.

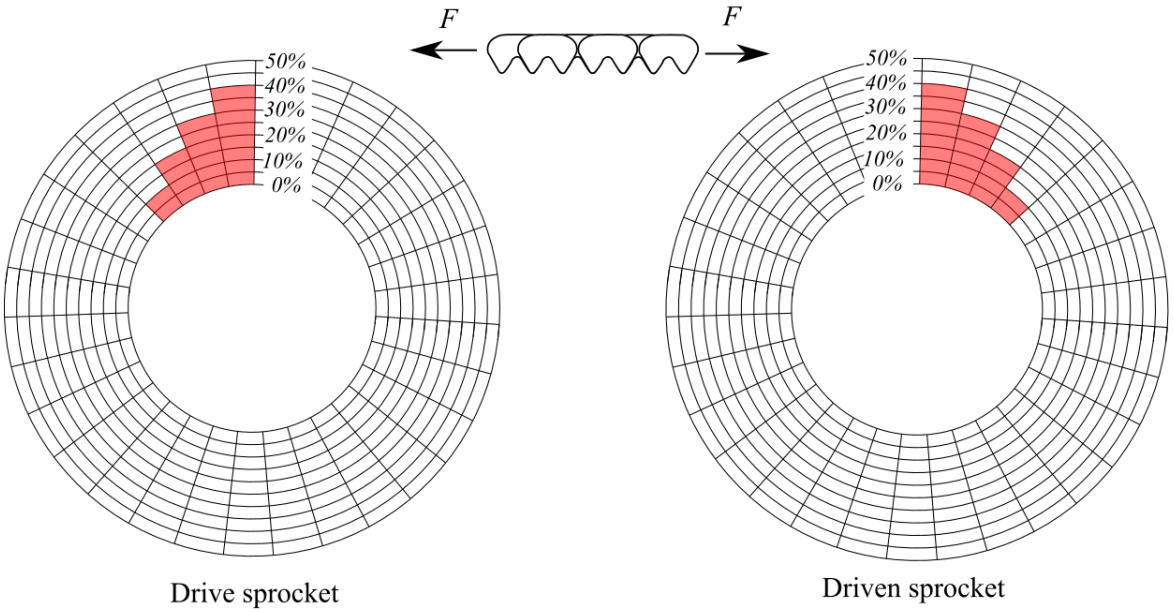

Figure 3. Load distribution between the teeth

In order to have a more accurate fatigue model of the sprockets, it is desired to find the real load distribution between the teeth. This will serve as the base for a fatigue calculation, and with these result, the possibility of changing the production of the sprockets to PM will be investigated by BorgWarner. Even with a small saving per sprocket will yield a large annual saving as the production volume is substantial.

3. Chain model

The simulation of the sprocket set and the chain was done in ADAMS machinery. In figure 4, the model is shown.

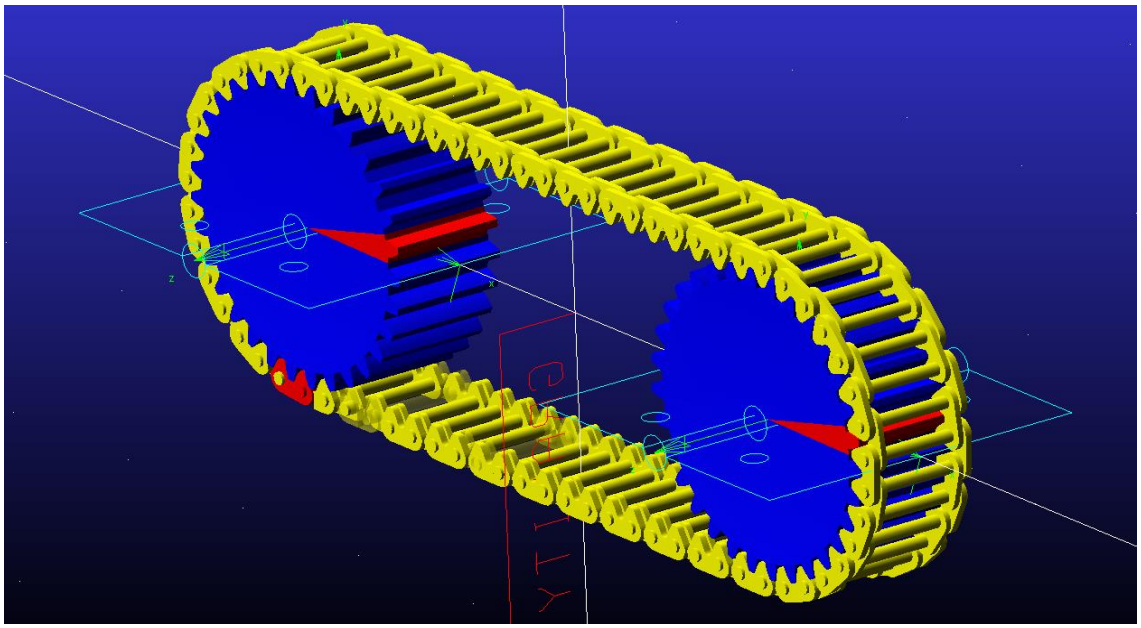

Figure 4. Simulation model in ADAMS Machinery

3.1 Approximative calculation by hand

In order to estimate the plausibility of the simulation output, a brief hand calculation based on the approximated load distribution was made.
Given the sprocket with the pitch radius of 46.994 mm and the applied torque M Nm, the approximate chain tension can be calculated as

$$F = \frac{M}{46.994 * 10^{-3}} \ N \qquad (1)$$

which can be seen in figure 5.

With the torque ranging from 0-1500 Nm, the expected chain tension should be in the range of 0-32000 N.

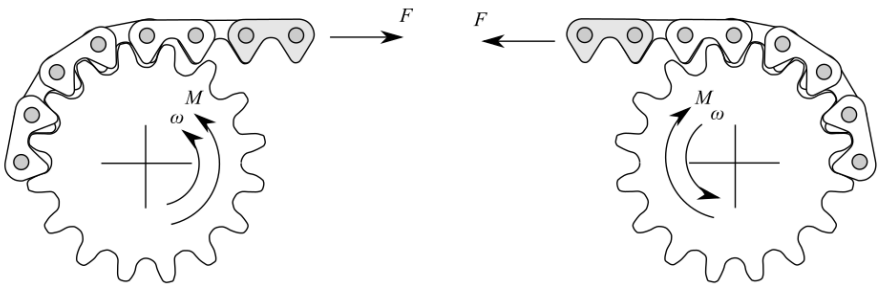

Figure 5. Chain tension with applied torque

3.2 Approximative sprocket design

The chain employed in the D7a application is of the type Hy-Vo, which uses rocker-pins as connectors, adding degrees of freedom and thus making the chain more complex than the usual silent chain, see figure 6. ADAMS Machinery only supports silent chains with regular pins, which can be seen in figure 7, altering the behavior of the chain. Morse Tec, however, provided an approximative design of the chain profile which would be comparable with the real Hy-Vo profile, but with ordinary pins.

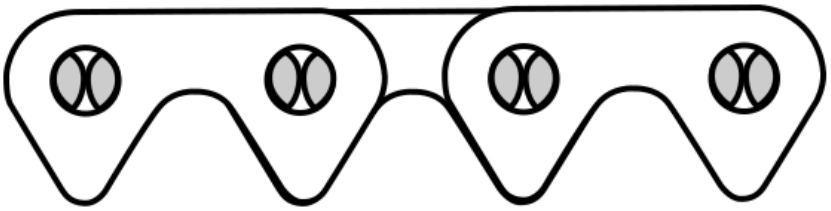

Figure 6. Hy-Vo links with rocker-pins

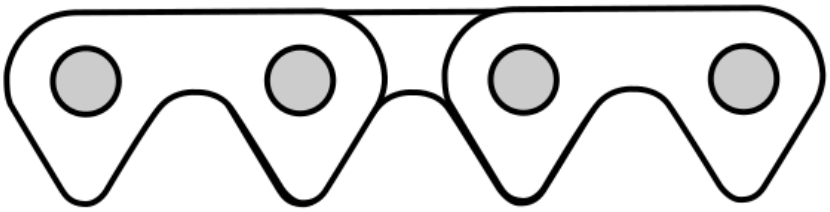

Figure 7. Traditional links with ordinary pins

However, it was not possible to simulate this Hy-Vo chain and sprocket geometry in the ADAMS chain module. Possible explanations might be the limitations of the geometry input of the chain module. Two sources of error were identified. First, possible limitations to the basic rack geometry. Second, the large negative addendum correction modification is not accepted, the reference diameter is large compared to the sprocket outer diameter. The latter was confirmed with technical support at MSC who provides the software.

In order to be able to use ADAMS for chain simulation, a new sprocket and chain geometry was needed, obviously, a design very close to the original design. In attempt to find a design that would be accepted as an input to ADAMS, the default ADAMS geometry was used as a basis, see table 1.

	Symbol	Unit	ADAMS default geometry	Real design
Sprocket width	b	mm	10	33.87
Number of teeth	z	-	34	31
Pitch diameter	D	mm	68.72	93.989
Root diameter	D_{bot}	mm	60.11	76.358
Tip diameter	D_{tip}	mm	66.78	87.945
Pressure angle	α_t	deg	30	28
Over pin diameter	L	mm	70.18	88.995
Pin diameter	r	mm	4.0	5.225

Table 1. The design parameters for the sprockets in ADAMS and the real, respectively.

First, the module was identified by using the reference diameter and number of teeth

$$m = \frac{D}{z} = \frac{68{,}72}{34} = 2.021 \text{ mm} \quad (2)$$

The base circle radius is

$$g = \frac{D}{2}\cos(\alpha) = \frac{68.72}{2}\cos(30) = 29.756 \text{ mm} \quad (2)$$

To find the addendum correction factor, x, the relation between the addendum correction and the dimension over pins was used. For a detailed description of each step, the reader is referred to Vedmar, 2013 [3].
For a sprocket with an even number of teeth, the distance over pins can be written as

$$L = 2 * (r + \rho) \quad (3)$$

which can be seen in figure 8.

Solving for ρ yields

$$\rho = \frac{L}{2} - r = \frac{70.18}{2} - \frac{4}{2} = 33.09\text{mm} \quad (4)$$

With the relationship

$$\rho = \frac{g}{\cos(\Psi)} \rightarrow \Psi = \cos^{-1}\left(\frac{g}{\rho}\right) = 25.94^{o} \quad (5)$$

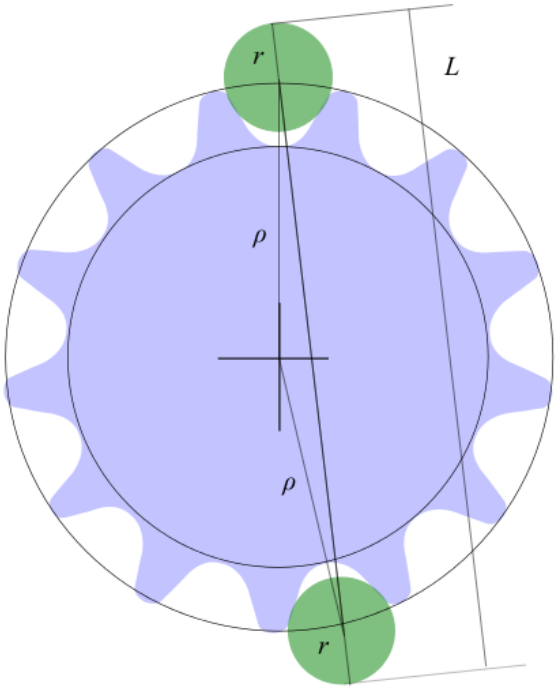

Figure 8. Measurement over pins

The addendum correction factor (figure 9) can be calculated from

$$\text{inv}(\Psi) = \frac{r}{g} - \frac{\pi}{z} + \frac{\pi + 4x\tan(\alpha_t)}{2z} + \text{inv}(\alpha_t) \quad (6)$$

Solving for x yields

$$x = \frac{2z\left(\frac{\pi}{z} - \frac{r}{g} + \text{inv}(\Psi) - \text{inv}(\alpha_t)\right) - \pi}{4\tan(\alpha_t)} = -1.209 \quad (7)$$

That is, the addendum correction factor of the default design is x=-1.209. The rack addendum factor and dedendum factor can then be found by

$$\frac{D_{tip}}{2} = m\left(\frac{z}{2} + x + h_{0a}\right) \rightarrow h_{0a} = \frac{D_{tip}}{2m} - \frac{z}{2} - x = 0.729 \quad (8)$$

and

$$\frac{D_{bot}}{2} = m\left(\frac{z}{2} + x - h_{0d}\right) \rightarrow h_{0d} = -\frac{D_{bot}}{2m} + \frac{z}{2} + x = 0.921 \quad (9)$$

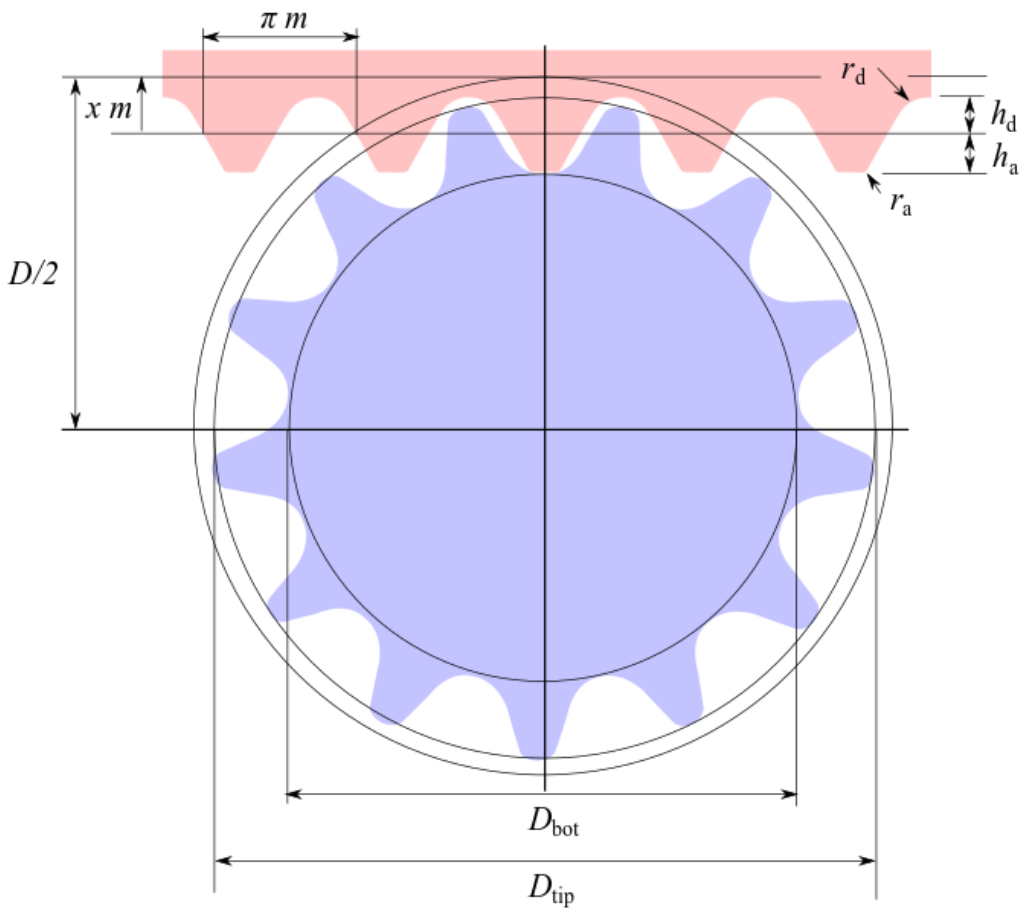

Figure 9. Sprocket measurements, rack addendum

As the basic rack is now known, a new design is developed based on this rack but adopted to the original design, a design with the module m=3.032 mm and 31 teeth. For this design the pitch diameter can be calculated as

$$R_t = \frac{mz}{2} = 46.995\ \text{mm} \rightarrow D = 93.989\ \text{mm} \quad (10)$$

And the base circle radius as

$$g = R_t \cos(30^0) = 40.70\ \text{mm} \quad (11)$$

The top and bottom diameters can be calculated as

$$D_{tip} = 2m\left(\frac{z}{2} + x + h_{0a}\right) = 91.078\ \text{mm} \quad (12)$$

$$D_{bot} = 2m\left(\frac{z}{2} + x - h_{0d}\right) = 81.072\ \text{mm} \quad (13)$$

Obviously, the dimension over pins will not be the same for the adopted design as for the other designs, and must be determined. Using the pin diameter of 5.000 mm yields

$$\text{inv}(\Psi) = \frac{r}{g} - \frac{\pi}{z} + \frac{\pi + 4x\tan(\alpha_t)}{2z} + \text{inv}(\alpha_t) = 0.019 \rightarrow \Psi = 21.79^o \quad (14)$$

$$\rho = \frac{g}{\cos(\Psi)} = \frac{40.70}{\cos(21.79^0)} = 43.83 \text{ mm} \quad (15)$$

And the dimension over pins with an odd number of teeth can be calculated as

$$L = 2r + \rho\sqrt{2(1 - \cos\left(\pi\frac{z+1}{z}\right))} = 92.548 \text{ mm} \quad (16)$$

With all the required design parameters calculated, a brief comparison can be made, see table 2.

	Symbol	**Unit**	**Real design**	**Approximated design**
Sprocket width	b	mm	33	33
Number of teeth	z	-	31	31
Pitch diameter	D	mm	93.989	93.989
Root diameter	D_{bot}	mm	76.358	81.072
Tip diameter	D_{tip}	mm	87.945	91.078
Pressure angle	α_t	deg	30	30
Over pin diameter	L	mm	88.995	92.5475
Pin diameter	r	mm	5.225	5.000

Table 2. The design parameters for the real design and the approximated design, respectively.

For the chain link geometry, the size was also required to change to fit the new set of sprockets. With the same rack used in both sets, the only change was to use a scale factor for the links. Using the module for each sprockets, this factor was set to

$$f = \frac{m_{new}}{m_{old}} = \frac{3.032}{2.021} = 1.500 \quad (17)$$

3.3 Simulation settings

The multi-body simulation of the system is dynamic. Simulations of dynamics systems rarely convergence if motions are applied instantly, by using e.g. a Heaviside function, see Figure 10. In order for the calculations to converge a smooth initiation of speed and torque is needed. In ADAMS a STEP-function is used, where both speed and torque are smoothly applied to the system, with a ramp-up time of 0.5 seconds. This curve is C^2-continuous, see figure 10, instead of the C^{-1} discontinuous Heaviside function.

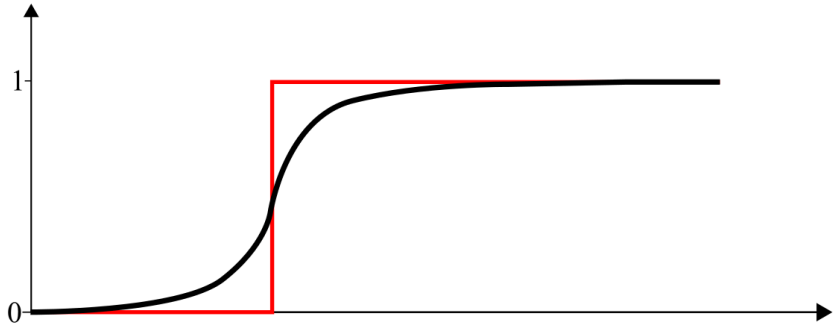

Figure 10. STEP function (black) and Heaviside step function (red)

The simulation type was dynamic and the integrator employed was the HHT, short for Hilber-Hughes-Taylor, which is used for integrating the equations of motion.
The integral error allowed was set to 1E-10 and the maximum time step the integrator is allowed to take, $H_{max,}$ was set to 1E-7.

For the materials, the most appropriate was to use the data from forged iron which was a standard material in ADAMS. The other settings was set to default.
For the chain, the stiffness and mass was provided by Morse TEC and the inertia was calculated in CREO. By drawing the link and adding the desired width per link, the inertia was found.

3.4 Simulation delimitations

The simulations in ADAMS are very complex and time consuming. The average time spent on a single simulation was in the range of two days, thus making it necessary to limit the amount of simulations, i.e. limit variations in the input. Provided from the customer is a load chart spectrum, which consists of several different load situations, i.e. torque and rotational speed levels. Altogether, the load spectrum consists of 63 different combinations, which would take several months to make complete simulations. In order to have valid data for all the levels, but having a realistic simulation time, the input was set to 500, 1000, 1500 rpm and 500, 1000 and 1500 Nm with all combinations simulated. Showing a consistency in the load distribution and expected chain tension, it was reliable enough to interpolate the results to include the whole load spectrum.

One other aspect of interest is the performance after a certain time of usage, i.e. when the chain is slightly worn. Usually when a chain is worn, the chain links are elongated increasing the length of the chain. The chain is specified to have a maximum of 0.3 percent elongation after the full load spectra has passed. This might lead to a change in the load distribution over the sprocket over time, and for fatigue calculation, this is of vital importance.

However, this big increase in elongation was not supported in ADAMS. The maximum increase was set to 0.2% in order for the simulation to work. In order to obtain reliable result, several different combinations were simulated; 500 and 1500 rpm, 500 and 1500 Nm, 0.1% and 0.2% elongation. Thus, eight different combinations was simulated.

3.5 Simulation result

The following graphical results are for 500 rpm and 500 Nm. For the full result graphics, see appendix 1. Since the rotational speed and the applied torque is ramped from zero at start to maximum after 0.5 seconds, the graphs have only a valid range after 0.5 seconds.

3.5.1 Chain tension

The tension in the chain is as expected circa the torque divided by the active radius. Going from the active side with full tension, through the drive sprocket to the slack side, where there is no tension, the chain experiences big differences in tension, see figure 11. Seen from the figure is also the steady decreasing from full tension to no tension. This is because the load distribution; the further into the drive sprocket, less contact forces are present on the teeth and thus, less chain tension. The tension is increasing linearly with the applied torque, as expected, see table 3.

Rpm \ Torque (Nm)	500	1000	1500
500	10882 N	21850 N	32400 N
1000	10900 N	21920 N	33600 N
1500	11120 N	22010 N	32600 N

Table 3. The maximum chain tension in different setups

The tension is as seen increasing slightly with the rotational speed. There is not enough data to make any certain conclusions, but the increase is probably related to the centrifugal force in the chain which arises from higher rotational speed. However, the increase is so small and the rotational speeds are relatively low and close to each other which make further investigation regarding the impact unnecessary.

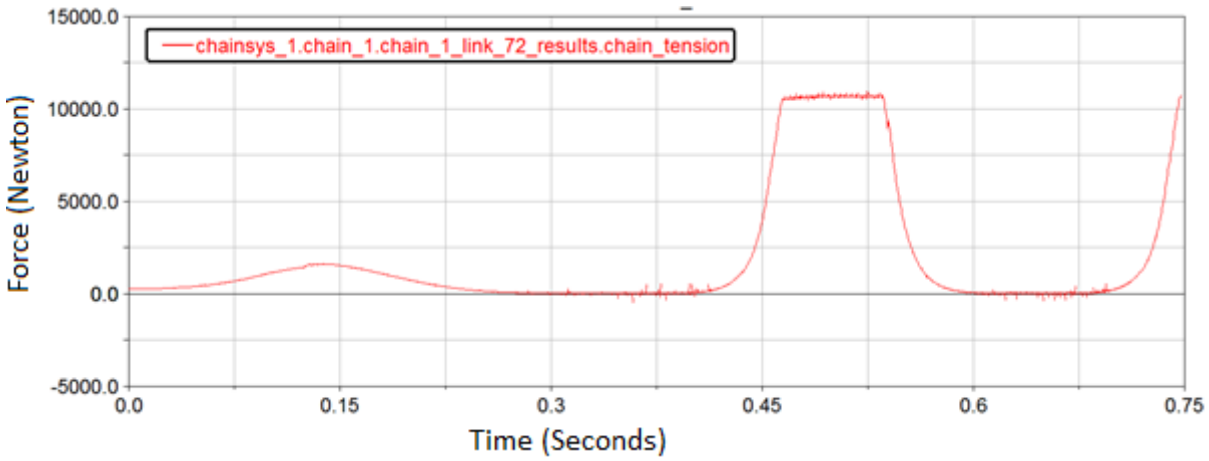

Figure 11. Chain tension as a function of time

3.5.2 Contact force

The contact force between the tooth and the chain changes as expected as the sprockets revolve. When the tooth engages in the drive side, the peak value of the contact force is found and is then decreasing steadily until the tooth is no longer in contact with the chain. For the driven sprocket, the contact force is steadily increasing from engagement to disengagement, with peak contact force just before the latter. Consult figure 12 and 13 for graphical result and table 4 for numerical result.

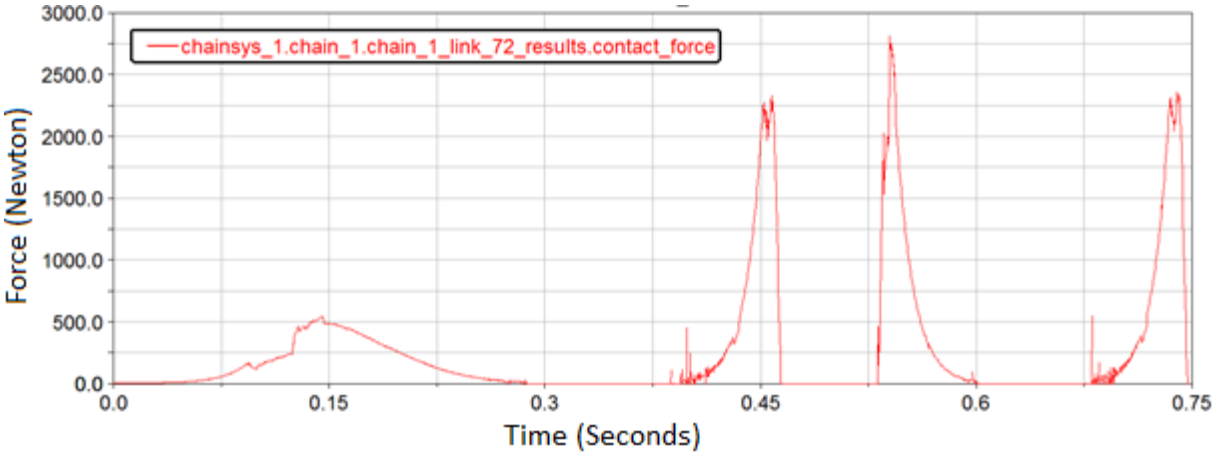

Figure 12. Contact force from t=0 to t=0.75

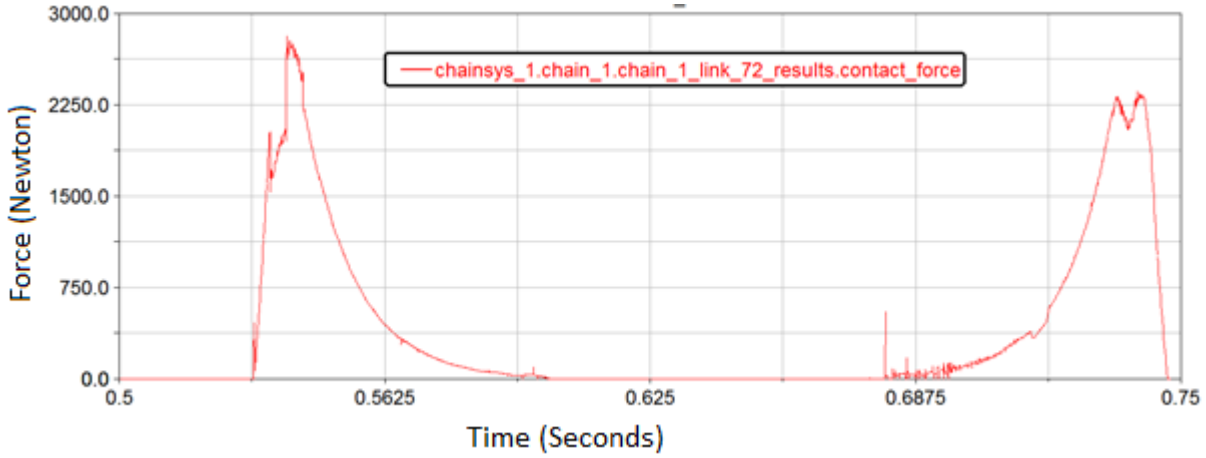

Figure 13. Contact force from t=0.5 to t=0.75

Rpm \ Torque (Nm)	500	1000	1500
500	2815 N	6021 N	9455 N
1000	3060 N	5320 N	8480 N
1500	3120 N	5420 N	8330 N

Table 4. The maximum contact force on a single tooth for different setups

3.5.3 Load distribution

The result obtained from the simulation is given as which percentage of the load one tooth experiences at its maximum, see table 5. The percentage is defined as the highest contact force throughout the engagement divided by the total chain tension.

Rpm \ Torque (Nm)	500	1000	1500
500	25.87%	27.56%	29.18%
1000	28.07%	24.27%	25.24%
1500	28.06%	24.63%	25.55%

Table 5. The maximum percentage of the load on a single tooth for different setups

For full simulation graphics, see appendix 1.

3.5.4 Elongated chain result

The result from the elongated chain shows no negative impact on the load distribution

0.1 % elongation		
Rpm \ Torque (Nm)	500	1500
500	24.93%	25.96%
1500	26.37%	23.95%

Table 6. The maximum percentage of the load on a single tooth for different setups with the chain elongated 0.1%

0.2 % elongation		
Rpm \ Torque (Nm)	500	1500
500	25.53%	24.94%
1500	26.46%	26.51%

Table 7. The maximum percentage of the load on a single tooth for different setups with the chain elongated 0.2%

From table 6 and 7, it is obvious compared to table 5 that the maximum percentage does not increase when the chain is elongated.

3.5.5 Real load variation between the teeth

As mentioned, the estimated load distribution between the teeth today was 40%-30%-20%-10%. From the ADAMS simulation, the real distribution can be calculated. Using the fact that roughly 15 teeth are in engagement with the chain and dividing plot into 15 sections, each section represent a tooth at a certain position, see figure 14. The intersection between the line that represent a tooth and the line that represents the continuous contact force gives the contact force a tooth experiences.

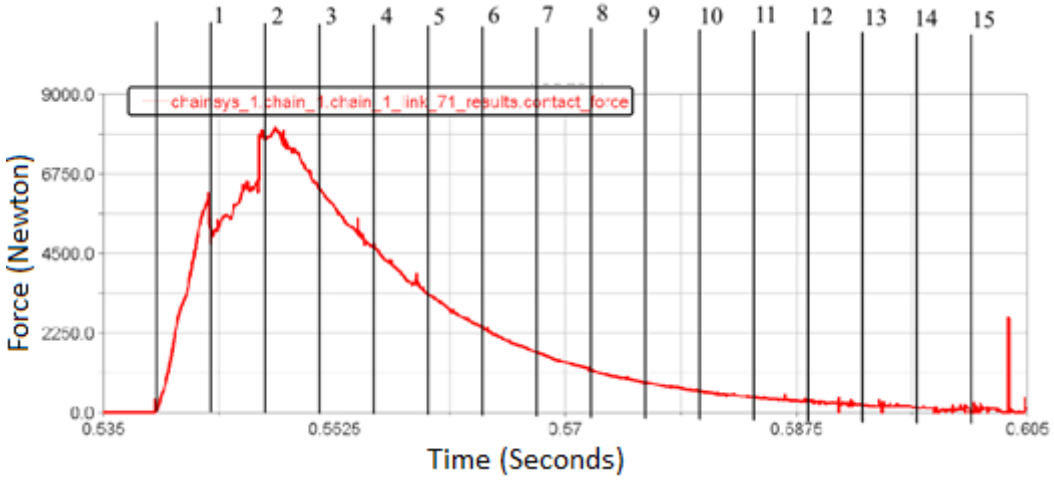

Figure 14. Load distribution for each tooth

Using the same approach as calculating the maximum load distribution yields

Tooth	Percentage of total load	Previous estimation
1	18	40
2	25	30
3	19	20
4	12	10
5	10	0
6	6	0
7	4	0
8	3	0
9	2	0
10	1	0
11-15	<1	0

Table 8. Real load distribution and estimated load distribution

Seen in table 8, the true load distribution has more teeth engaged and operates at lower force levels. Tough these results are valid for only one torque/rotational speed combination, it can represent the general distribution roughly. Worth noting, the first tooth carries the third greatest load, and not the greatest as in the estimation. This has, however, not an impact on the expected life, but it is worth noting. Also, the driven sprocket might differ from the drive sprocket, but the difference is relatively small and the same load distribution can be used. The major difference was the peak force, which was generally around 5 percent greater in the drive sprocket.

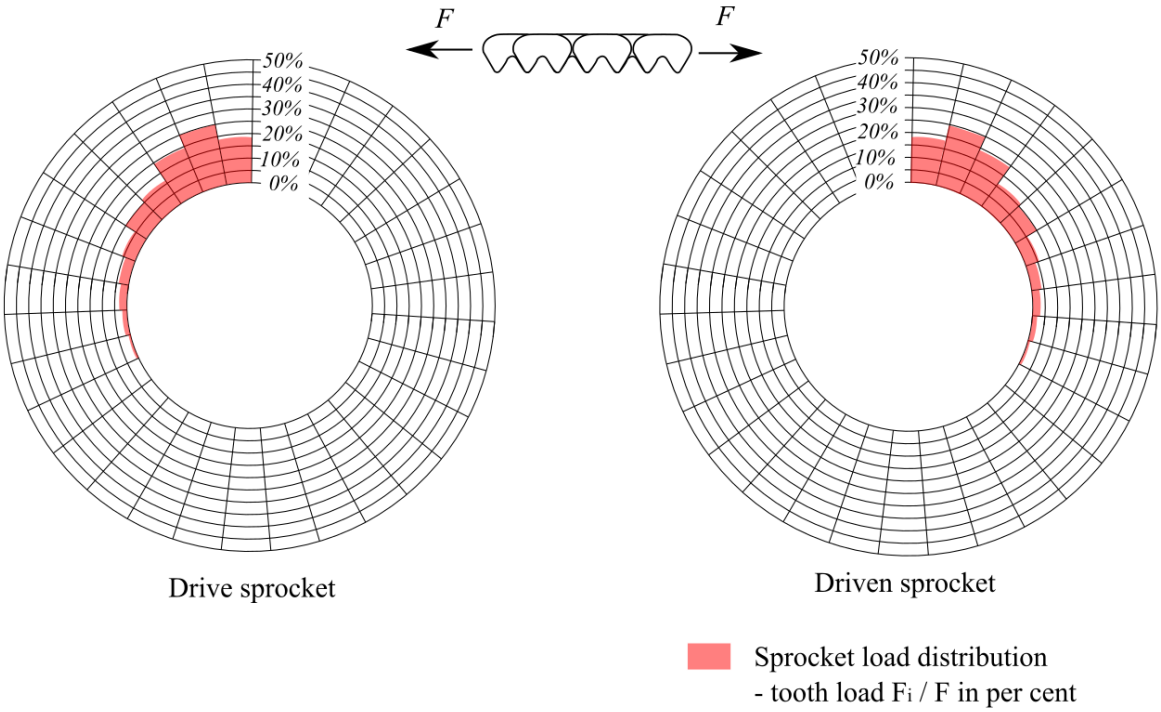

Figure 15. Real load distribution

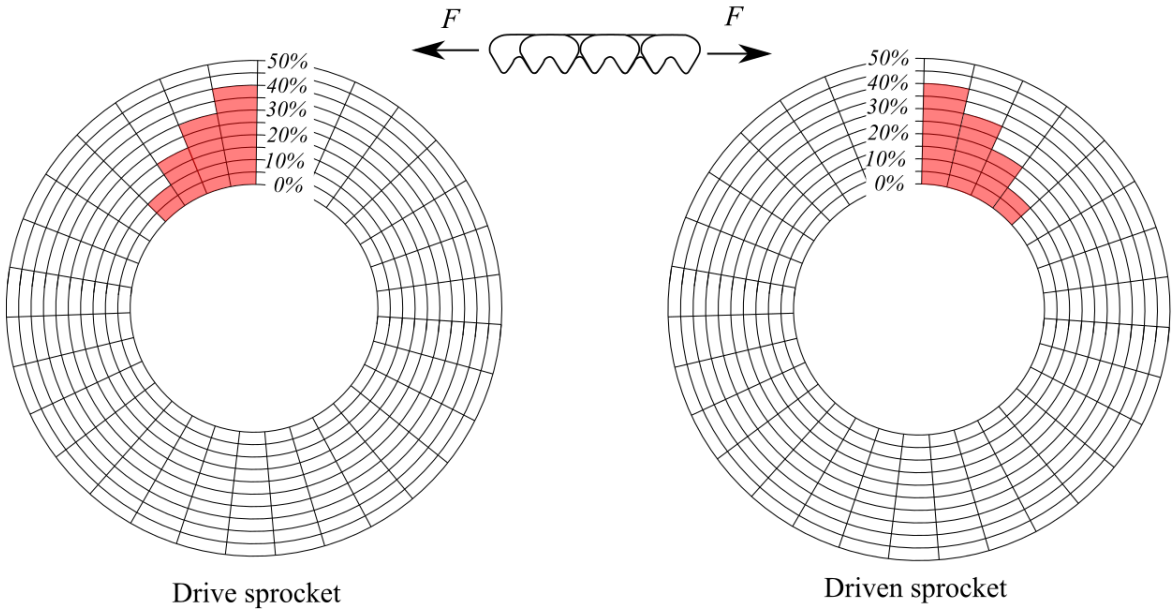

Figure 16. Estimated load distribution

Seen from figure 15 and 16, the differences are quite obvious. Not only are there more teeth engaged, but the loads are lower on each tooth, i.e. the percentage of the total load is lower.

4. Load on the teeth of the sprocket

With the load distribution between the sprockets known, the stresses in the sprockets can be calculated. The stresses of interest are the result from contact and bending, respectively, see figure 17. The bending stresses which arises in the root can be calculated using the cantilevered beam theory. This can be done in different ways, one described in ISO-6336 and a different approach described as Lewis parabolic tooth equivalent.

The stresses arising from contact can be calculated using the Hertzian contact theory.

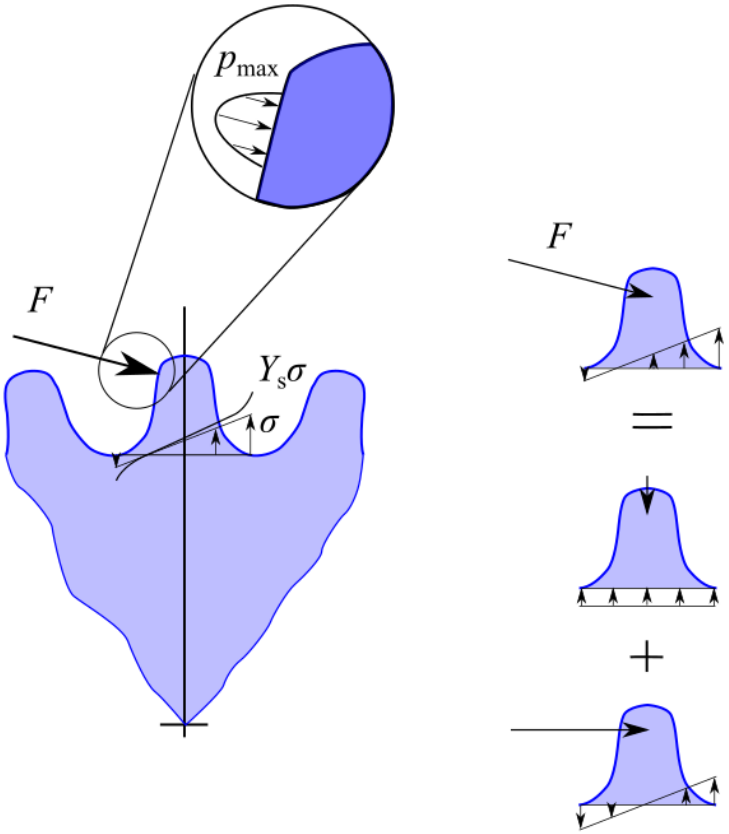

Figure 17. The loading on a tooth. The bending stress in the tooth and contact stress on the surface

Since the loading and geometry for the sprockets considered are similar to those for gears, the same standard and material data can be used. The ISO standard for gears can be found in ISO-6336; Calculation of load capacity of spur and helical gears.

4.1 Bending stresses

Seeing the loading on the tooth as an equivalent of the loading on a cantilevered beam, the geometry of the tooth has to be determined. First, the location of where the force is applied, and at what angle, has to be determined. Second, the width of the tooth at the root has to be determined.

4.1.1 Active profile

When a tooth is in engagement with the chain, the contact point on the tooth changes. The stresses in the root which arise from bending is affected by the leverage arm, and this changes as the contact point changes, see figure 18. The radius where the sprocket is in engagement can be calculated as

$$s = \sqrt{r^2 - g^2} \tag{18a}$$

$$s = g * \Psi \tag{19b}$$

$$\rightarrow (g * \Psi)^2 = r^2 - g^2 \rightarrow r^2 = g^2(1 + \Psi^2) \rightarrow r = g * \sqrt{1 + \Psi^2} \tag{19}$$

With the start of the active profile at $\Psi = 4.71$ deg and the tip break at $\Psi = 17.48$ deg, the radius of the contact varies between 41.634 mm and 43.382 mm.
Using the mean value will be sufficient for calculations

$$r_{contact} = \frac{r_{start} + r_{end}}{2} = 42.508\text{mm} \tag{20}$$

At this radius, the angle is calculated as

$$\Psi = \sqrt{\left(\frac{r}{g}\right)^2 - 1} = 12.74^o \tag{21}$$

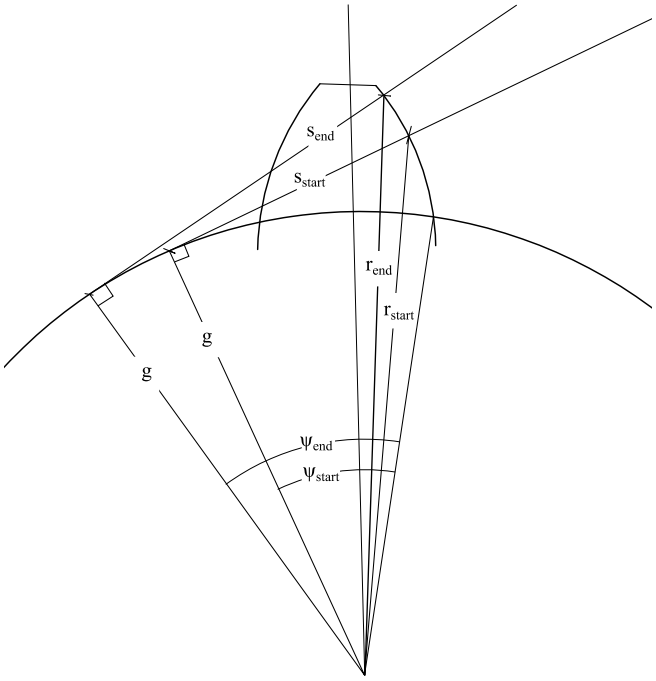

Figure 18. Calculation of the active profile

4.1.2 Tooth thickness and height

With the location of the load applied to the tooth known, the dimensions of the tooth has to be known in order to use the cantilevered beam theory. The stresses in the root will be affected by both the force applied, but also on the leverage arm and the thickness of the root. The radius of where the thickness of the root is calculated can be done in several different ways. In ISO-6336, the root stresses are considered at the 30 degree tangent to the central line.
One other way of determining the root stress is by using Lewis parabolic tooth equivalent instead of looking at stresses at the 30 degree tangent. These two methods yields for similar result, but Lewis method gives a higher stress level.
In this thesis, the ISO-6336 standard is used, thus the tooth thickness is determined at the 30 degree tangent. This can be found by calculations, or easier by graphical methods, for example, by the measurement tool in CREO, see figure 19.

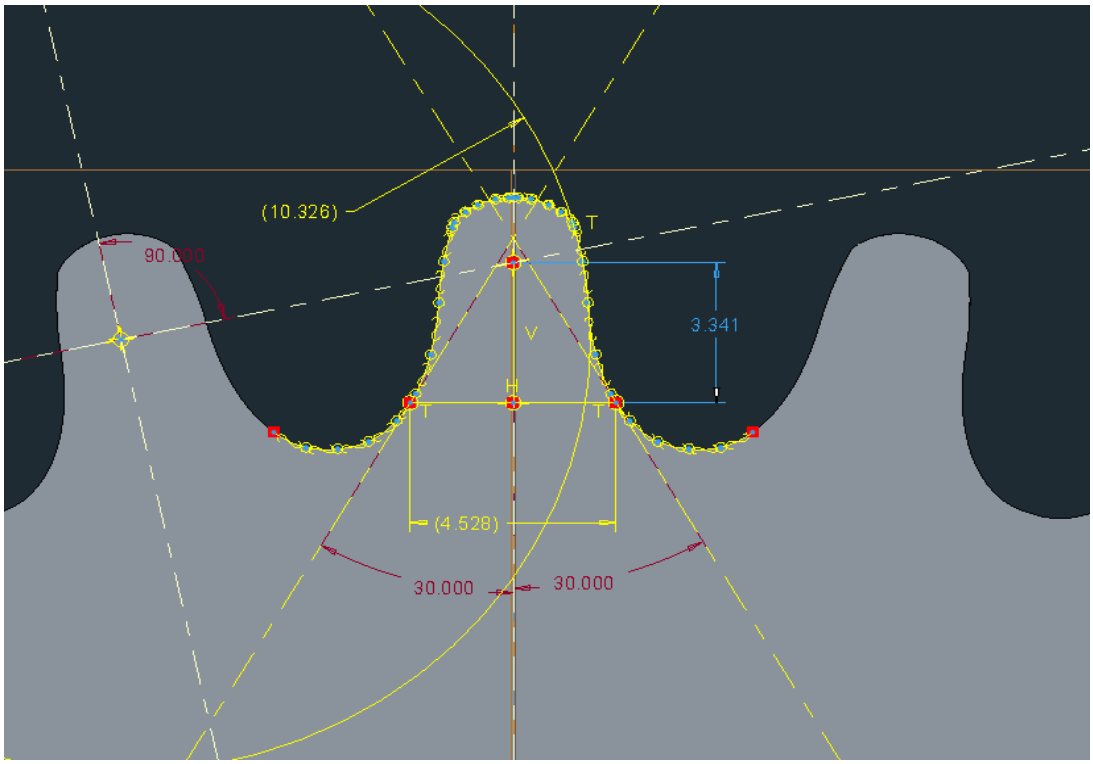

Figure 19. Measurement in CREO

The thickness of the tooth at the root, s, and the height of the tooth, h, can also be found by the measurement tool and are

s = 4.528 mm
h = 3.341 mm

4.1.3 Bending stresses in the root

With the loading and the geometry known, the stresses in the tooth can be calculated. The stresses in the sprocket which arise from applying load on its teeth are greatest in the root, see figure 20. The coast side is always exposed of higher stress levels than the load side because of the angle which the load is applied. However, this is not usually considered when calculating the stresses in the tooth, and it is not part of the ISO way of procedure.

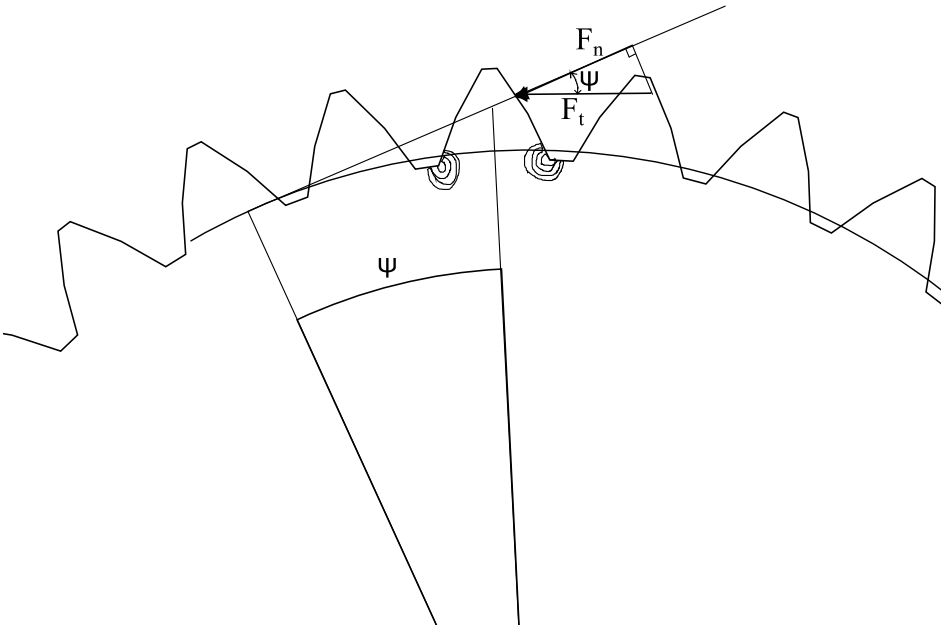

Figure 20. Bending stresses in the root

The tooth root stress, according to ISO 6336-3, is given as [4]

$$\sigma_{F0} = \frac{F_t}{bm} Y_f Y_S Y_\beta Y_B Y_{DT} \quad (22)$$

where Y_B , Y_{DT} and Y_β is set to 1, given the geometry.

4.1.4 Form factor, Y_f

Y_f is calculated from the cantilever beam theory, which can be applied to the tooth of a sprocket. It says that the nominal stress can be calculated as [4]

$$\sigma = \frac{F_n \cos(\psi) h}{\frac{bs^2}{6}} = \frac{F_n}{b}\frac{6h}{s^2}\cos(\psi) = \frac{F_n}{bM}\frac{6\frac{h}{m}}{\left(\frac{s}{m}\right)^2}\cos(\psi) \quad (23)$$

which can be compared to σ_{F0}, and with $F_t = F_n \cos(\alpha_t)$, giving that

$$Y_f = \frac{6\frac{h}{m}}{\left(\frac{s}{m}\right)^2}\frac{\cos(\psi)}{\cos(\alpha_t)} = 3.275 \quad (24)$$

4.1.5 Stress correction factor, Y_S

The stress correction factor is used to convert the nominal tooth root stress to a local root stress. In general, a stress amplifying effect is observed in the root which the stress correction factor corrects for.
In accordance with equation 36 in ISO 6336-3, this stress amplifying factor can be calculated via [4]

$$Y_s = (1.2 + 0.12\frac{S_{Fn}}{h_{Fe}})q_s^{\left[\frac{1}{1.21+\frac{2.3}{\frac{S_{Fn}}{h_{Fe}}}}\right]} \quad (25)$$

Where

$$q_s = \frac{S_{Fn}}{2\rho_F} \quad (26)$$

Using CREO for measuring the radius of the root rather than the numerical calculation yields for $\rho_F = 3.914mm$. Inserting the values yields

$$Y_s = \left(1.2 + 0.12 * \frac{4.528}{3.341}\right) * \frac{4.528}{2*3.914}^{\left[\frac{1}{1.21+\frac{2.3}{\frac{4.528}{3.341}}}\right]} = 1.129 \quad (27)$$

However, this equation is only valid in the range of $1 < q_s < 8$. The radius of the root of the sprocket is large, which means that q_s is out of range at $q_s = 0.58$. Hence, the result cannot be used.
Without the possibility to calculate the stress correction factor from equation 28, FEM will be used instead. This will give the real stress in the tooth. By comparing this to the equation for the nominal tooth root stress, the difference between the results will be the stress correction factor.

The stress correction factor is geometry dependent and can therefore be calculated using unit force. Using the equation for the nominal tooth root stress, and inserting all the known values, only the stress concentration factor is unknown.

$$\sigma_{F0} = \frac{F_t}{bm} Y_f Y_S = \frac{F_t}{bm} * \frac{6\frac{h}{m}}{\left(\frac{s}{m}\right)^2} \frac{\cos(\psi)}{\cos(\alpha_t)} Y_S \quad (28)$$

which yields

$$Y_s = \frac{\sigma_{F0}}{\frac{F_t}{bm} * \frac{6\frac{h}{m}\cos(\psi)}{\left(\frac{s}{m}\right)^2 \cos(\alpha_t)}} \quad (29)$$

Here, the real stress is related to the applied force, leaving the stress concentration factor known.

4.1.5.1 FEM calculation

A STP-file with the sprocket was provided from BorgWarner. By altering the geometry in *SpaceClaim*, only a small part of the sprocket was used, see figure 21. The part was then meshed fairly coarse, see figure 22. By *refinement*, the desired tooth was meshed with smaller triangles at critical areas, in the root and at the location of where the force was applied, see figure 23 and 24.
The number of nodes added up to 125087 and number of elements 84716.

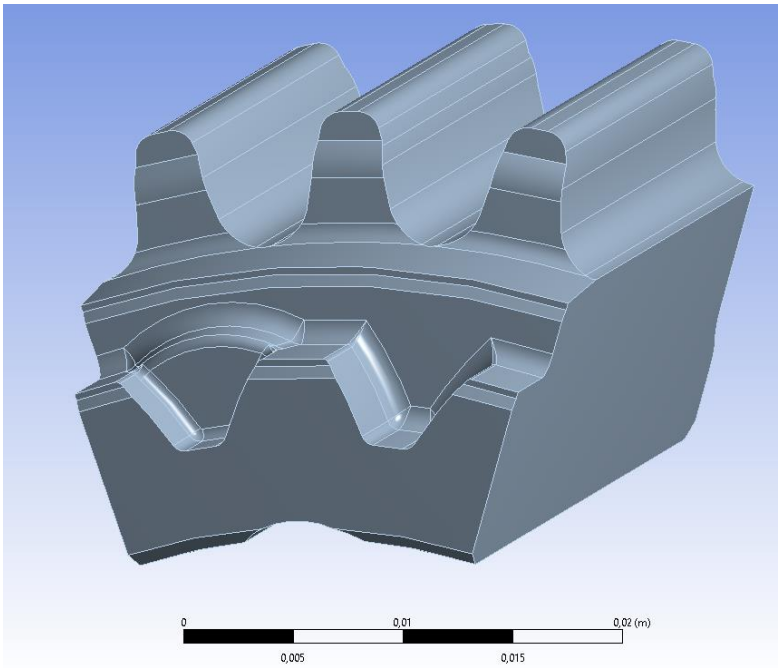

Figure 21. Part of model used in ANSYS to calculate the stress concentration factor

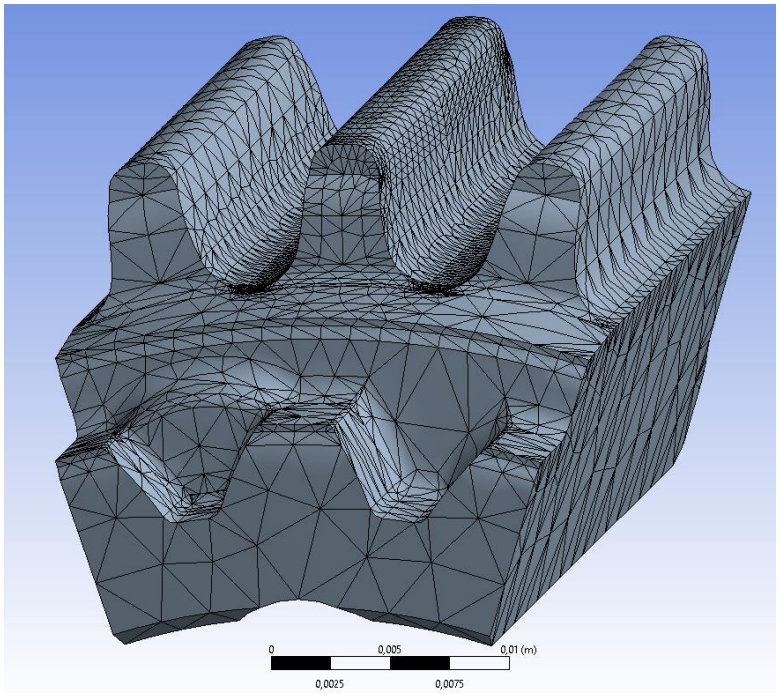

Figure 22. The mesh for the FEM calculation

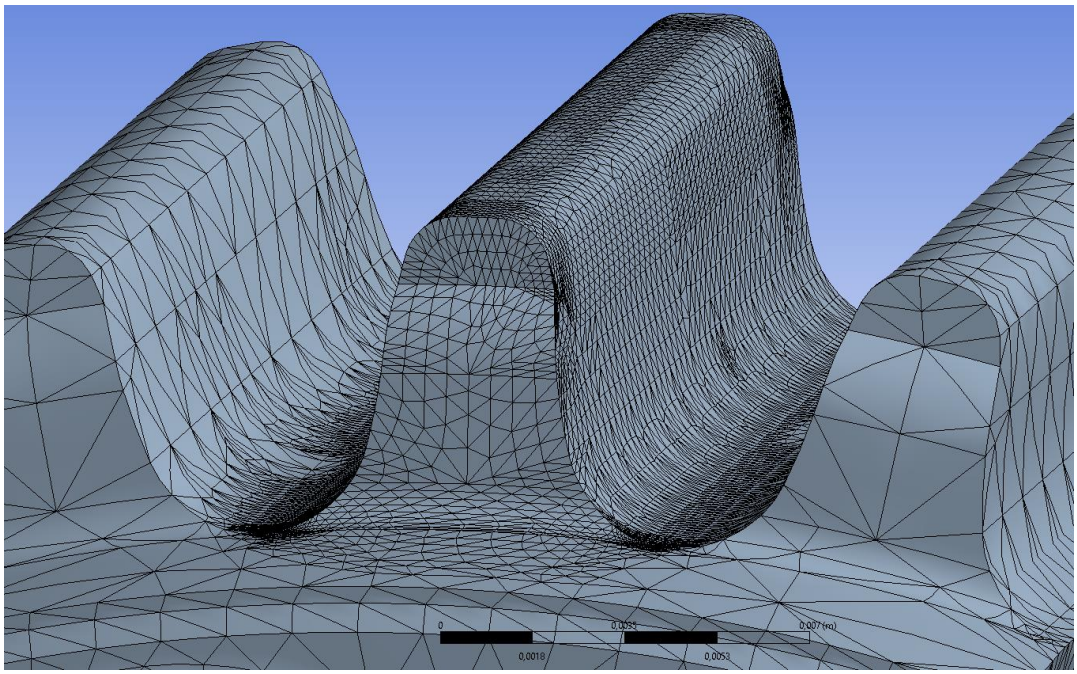

Figure 23. Close up on the surface of interest where the mesh is refined

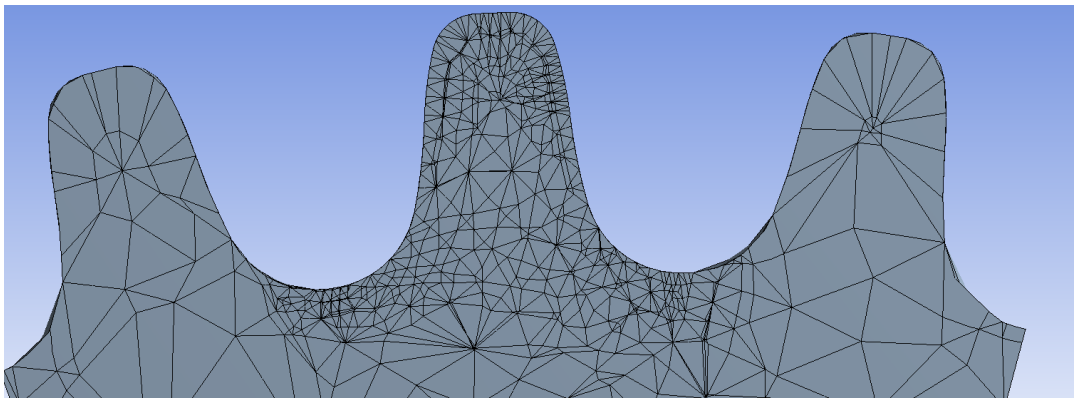

Figure 24. A section plane in the middle of the tooth with finer mesh around interesting areas, the root and where the load is applied

At the active radius, calculated in section 4.1.1, the area concerned was divided into two smaller areas with a straight line. This was done in *SpaceClaim* with the tool *Face Split*. This allows for the force to be applied along this line, distributing it evenly over the length of the tooth.

In order to get the force in the accurate direction, a local coordinate system was placed with the origin of x and y on the previously defined line. Then, the z axis was rotated so that the y axis touched the surface of the tooth, see figure 25. This was done by setting the "orientation about principal axis" to define by *Geometry Selection* and then use the defined line.
The two surfaces from the cut-off geometry were clamped with a *Fixed support*.

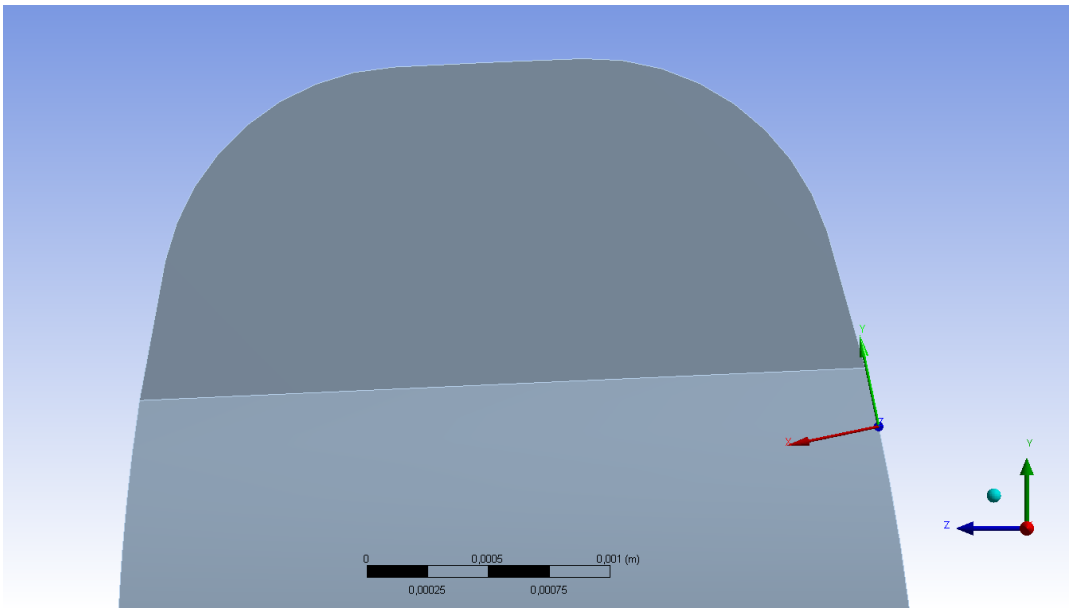

Figure 25. The definition of the local coordinate system

By applying a unit force of 10000N along the x axis of the new coordinate system (figure 26), the following stresses was found in the tooth

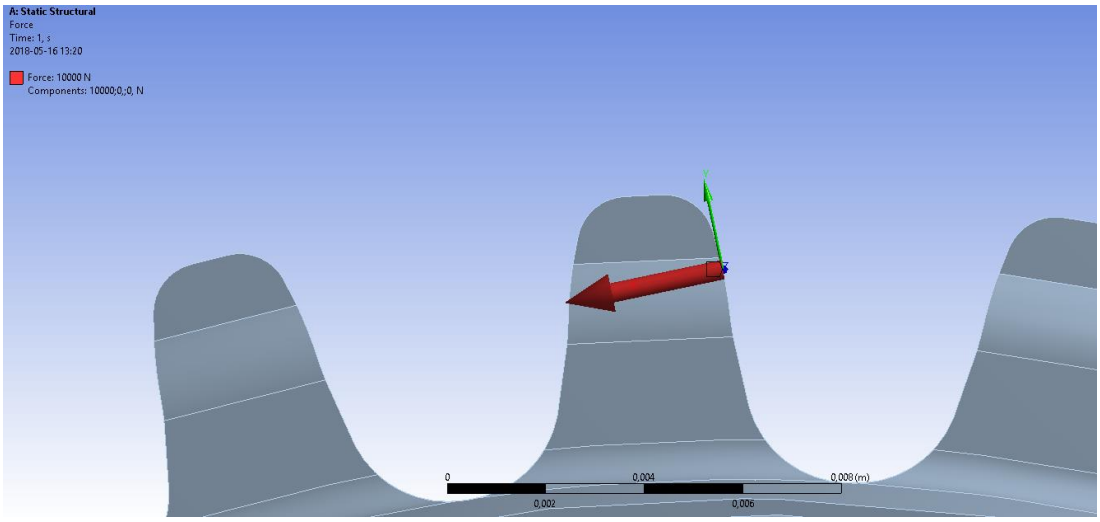

Figure 26. The force applied along the x-axis of the local coordinate system

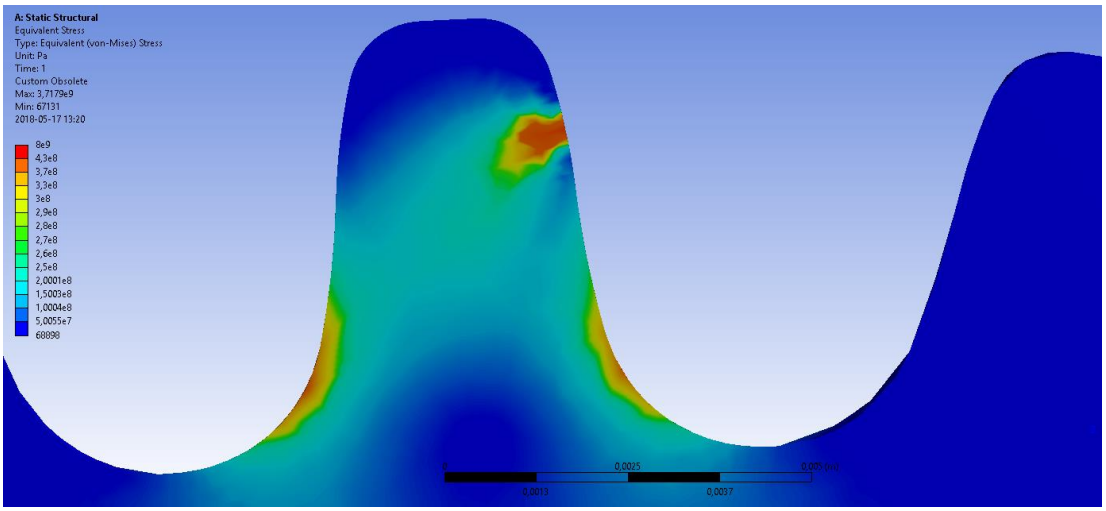

Figure 27. The graphical result from the FEM stress calculation

In order to avoid edge effects, a section plane was used in the middle of the sprocket, seen in the axial direction.
The maximum stresses in the root of the tooth was found to be 431.60 MPa, see figure 27. By adding even finer mesh around the area of the highest stress and recalculating, the maximum stress was found to be 431.97 MPa which verifies the result.
Using the formula for the stress correction factor and inserting the values from the first calculation yields

$$Y_s = \frac{\sigma_{F0}}{\frac{F_t}{bm} * \frac{6\frac{h}{m}\cos(\psi)}{\left(\frac{s}{m}\right)^2 \cos(\alpha_t)}} = \frac{431.60 * 10^6}{\frac{10000}{32.87 * 10^{-3} * 3.032} * \frac{6\frac{3.341 * 10^{-3}}{3.032}\cos(12.74)}{\left(\frac{4.528 * 10^{-3}}{3.032}\right)^2 \cos(28)}} = 1.347 \quad (30)$$

4.1.6 Application factor

The application factor, K_a, accounts for uncertainties in loads and impacts. The factor is determined by the operational behavior of the driving machine and the operational behavior of the driven machine, i.e. the torque input and the torque output in this case. There are four levels of operational behavior; uniform, moderate shocks, medium shocks and heavy shocks. Here, the application factor of 1.25 is used, which means that one of the axis experiences uniform operational behavior and the other moderate shocks.

4.1.7 Tooth root stress summary

With the load distribution known from the ADAMS simulation, the loading on the teeth needed to be known. Using the cantilevered beam theory and modifying the result by factors related to the geometry provided a formula in which the stresses in the tooth could be calculated given an applied force.

From ISO-6336, the formula is given as

$$\sigma_{F0} = \frac{F_t}{bm} Y_f Y_S \quad (31)$$

and with the usage of K_a yields

$$\sigma_{F0} = \frac{F_t}{bm} Y_f Y_S K_a \quad (32)$$

which with the values obtained gives

$$\sigma_{F0} = 55368 * F_t = 53950 * F_n \quad (33)$$

That is, for each newton applied to the tooth result in a maximum increase of 53950 Pa in the root of the tooth

4.2 Contact stresses

The stresses which arise in the contact between the chain and the sprocket can be calculated via the Hertzian contact stress theory. Using the formula for two cylindrical surfaces yields [5]

$$p_{max} = \sqrt{\frac{E^* F}{\pi b_{eff} R}} \; ; \; \frac{1}{R} = \frac{1}{\rho_1} + \frac{1}{\rho_2} \; ; \; \frac{1}{E^*} = \frac{1-v_1^2}{E_1} + \frac{1-v_2^2}{E_2} \qquad (34)$$

The contact surface of the chain can be approximated to a flat surface, which is equal to a cylinder with infinite radius, see figure 28. Using the same material with v=0.3 yields

$$p_{max} = \sqrt{\frac{1}{\pi * 2(1-v^2)}} \times \sqrt{\frac{EF}{b_{eff}} * \frac{1}{\rho_1}} = 0.418 * \sqrt{\frac{EF}{b_{eff}} * \frac{1}{\rho_1}} = 0.418 * \sqrt{\frac{210 * 10^9}{b_{eff}} * \frac{1}{\rho_1} F} \qquad (35)$$

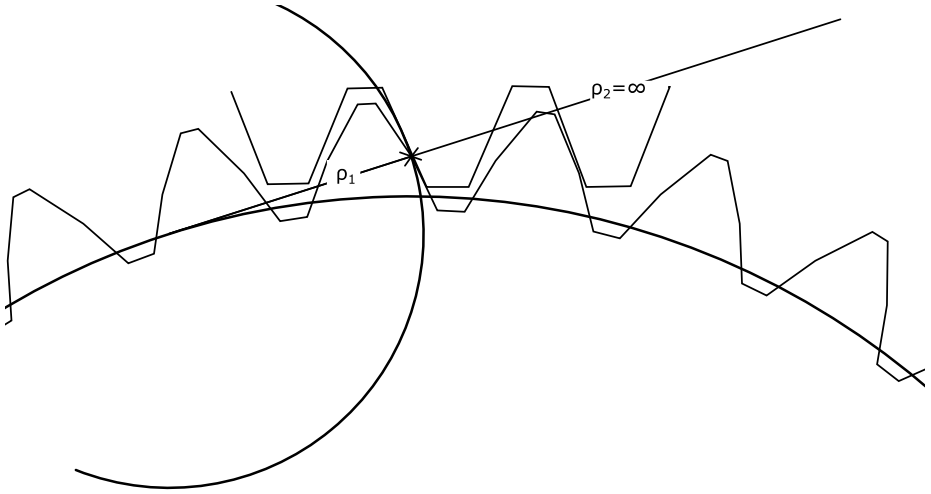

Figure 28. The radius for the Hertzian contact theory

Here, the radius of the tooth where it is in engagement can be taken directly from the 5.1.1 section. Since the tooth has an involute profile at the active profile, the radius of curvature is of the same magnitude as the arc of the circle defined by $s = g * \Psi$
With g = 41.497mm and Ψ=12.74 deg, the radius is 9.227 mm.

This yields

$$p_{max} = 1.99493 * \sqrt{\frac{F}{b_{eff}}} \text{ MPa} \qquad (36)$$

The effective length, b_{eff}, is defined as the number of links in contact with the sprocket multiplied with the length of each link, see figure 29. With a width of 1.55 mm per link, and with 11 links across the chain, the effective length was set to 17.05 mm.

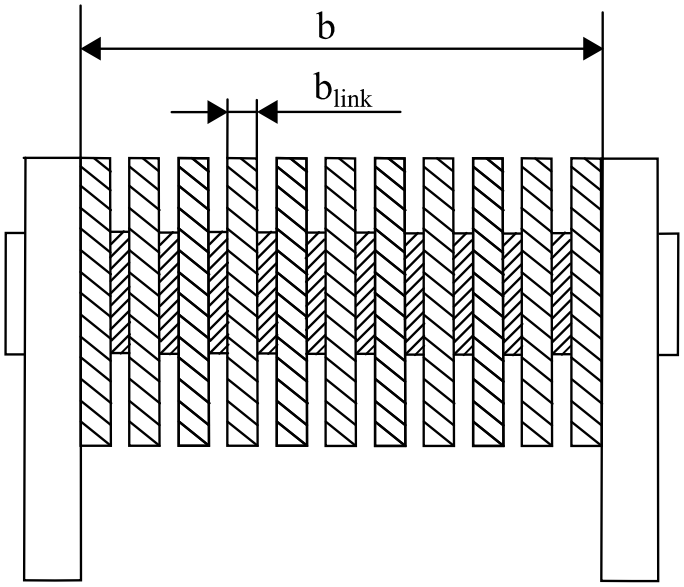

Figure 29. A link with its effective length

Thus, the maximum pressure can be written as

$$p_{max} = 15.28 * \sqrt{F}\ \text{MPa} \quad (37)$$

5. Sprocket fatigue

The D7-a application has a load spectrum which is dictating the mechanical life of the sprockets. This load spectra is confidential and can therefore not be part of this thesis with full specifications, but the distribution is depicted in figure 30. The interesting from this figure is the concentration of cycles in the low torque area, that it, the major part of the cycles is within the low range of the torque spectra. The total number of cycles with a torque level of higher than 1000 Nm is less than 200. The total number of cycles are well above one third of a billion. 7 percent of the cycles are at the lowest torque level, 25 Nm.

Seen in the graph is the torque plotted versus the number of cycles. The red symbolizes a positive torque input and the blue a negative torque input. That is, the sprocket is both used as the drive sprocket but also as a driven sprocket. That results in a change of drive and coast side, i.e. both sides of the tooth are used.

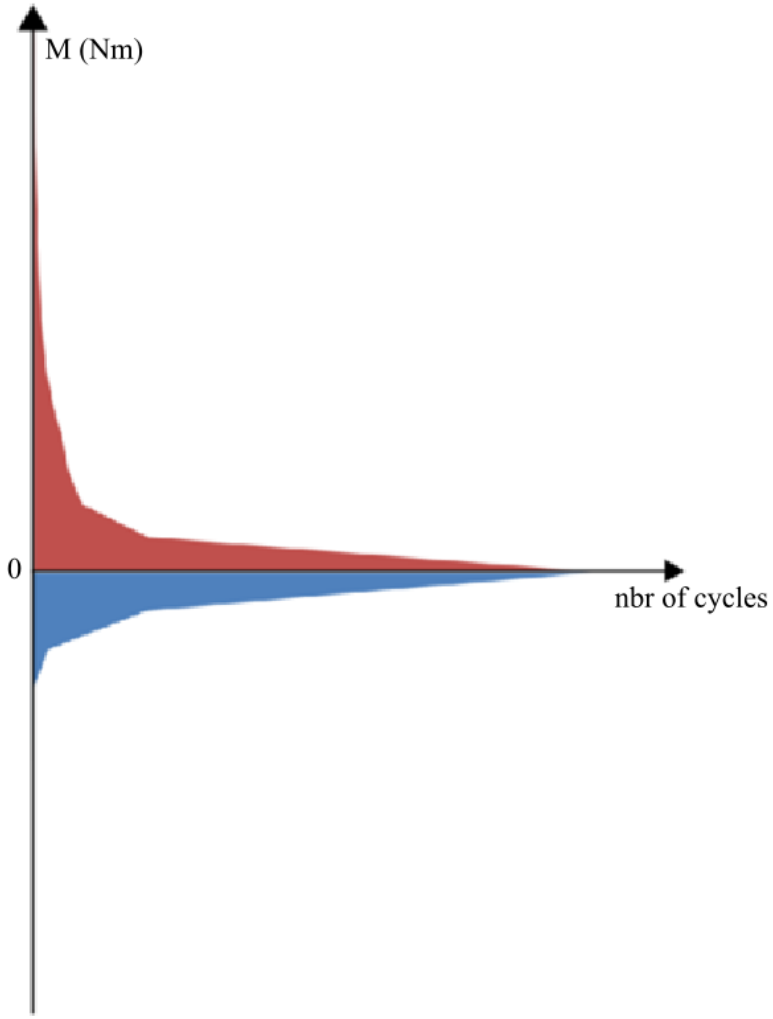

Figure 30. Load spectra for D7a

5.1 Fatigue calculation approach

By using the load spectrum and determine the maximum contact force for each combination, the maximum stress level in the sprocket can be calculated. Each stress level is applied for a number of cycles, also determined in the load spectrum.
From the simulations in ADAMS, a range of different load distribution was found. The range was between 24.3-29.2%, and in order to cover all possibilities, the fatigue calculation will be based on the maximum contact force of 30% of the chain tension. Worth noting, the general trend for the distribution was a decrease in maximum contact force when applying higher torque. That is, when maximum torque is applied, the contact force are more evenly spread over the tooth, making the maximum contact force slightly lower.
The impact from the elongated chain did not pose as an issue seen from the load distribution point of view and thus, further investigations are not needed.

5.2 Palmgren-Miner

Palmgren-Miner's rule on cumulative damage is the most widely used model for material failures caused by high-cycle fatigue. It states that for given stress levels and its corresponding number of cycles, material failure will occur when the damage fraction, c, reaches 1.
The loads in the considered sprocket are however not of that magnitude, but more cycles are applied. Using Palmgren-miners rule yields [7]

$$\sum_{i=0}^{k} \frac{n_i}{N_i} = c \tag{38}$$

When the damage fraction equals 1, failure occurs. The definition of failure is predetermined, meaning that the percentage of failures can be adjusted to meet certain requirements. A typical definition of failure is 1 percent, which means that 1 percent of the tests fails. In order to allow higher stresses, forces or other fail-causing quantities, the allowed percentage of failure can be increased.

5.3 S-N curve

A S-N curve is constructed in testing machines where different stress levels, S, are applied and the number of cycles to failure, N, are observed. This is one of the most common way of present fatigue data and is applicable for both bending and contact fatigue.

For case hardened wrought steels, the S-N curve and material data are found in ISO-6336:5, see table 9 and 10.
The lines 1-4 are used for different materials. In this case, line number 2 is used. The following points defines the S-N curve for contact and bending, respectively;

Contact	
S [MPa]	cycles
2400	1
2400	1e5
1500	5e7
1275	1e10

Table 9. Material data for the S-N curve, contact, case wrought hardened steel

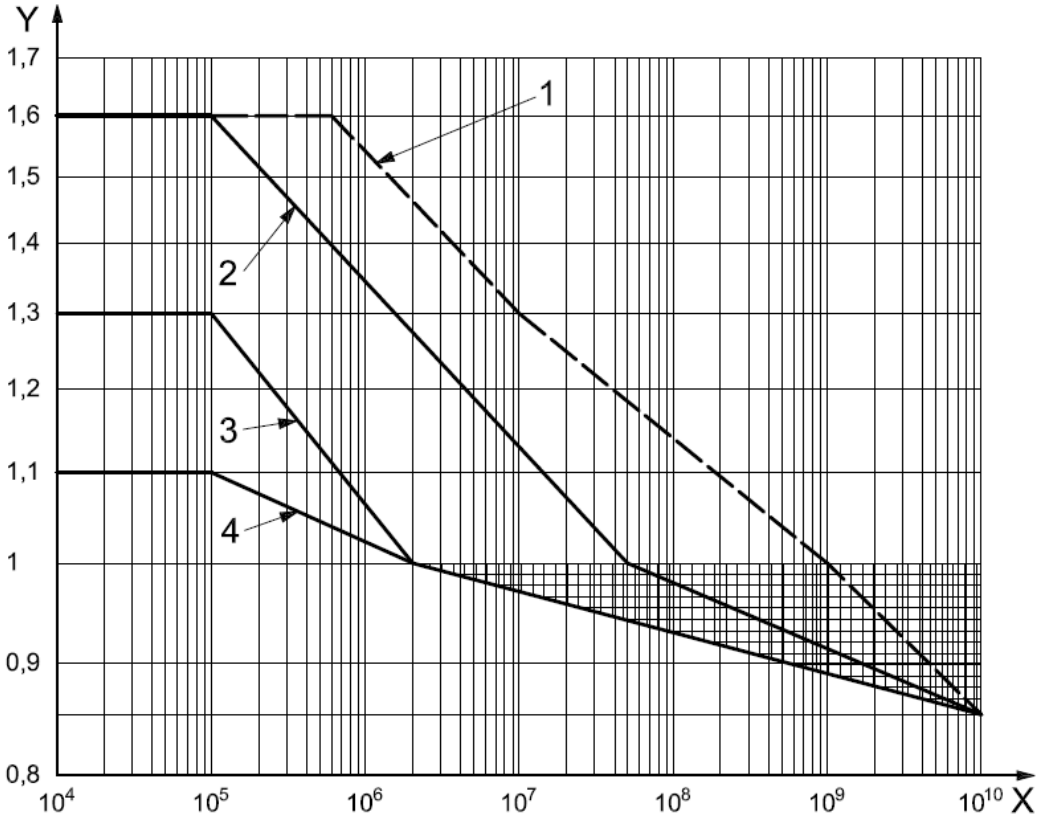

Figure 31. S-N curve for contact from ISO-6336

Seen in figure 31 is the S-N curve for contact, which is taken from ISO-6336:2. The y-axis represents the "life factor", which is a factor the stresses found from the material data is multiplied. The x-axis represents the number of cycles.

Bending	
S [MPa]	cycles
2300	1
2300	1e3
920	3e6
782	1e10

Table 10. Material data for the S-N curve, bending, case wrought hardened steel

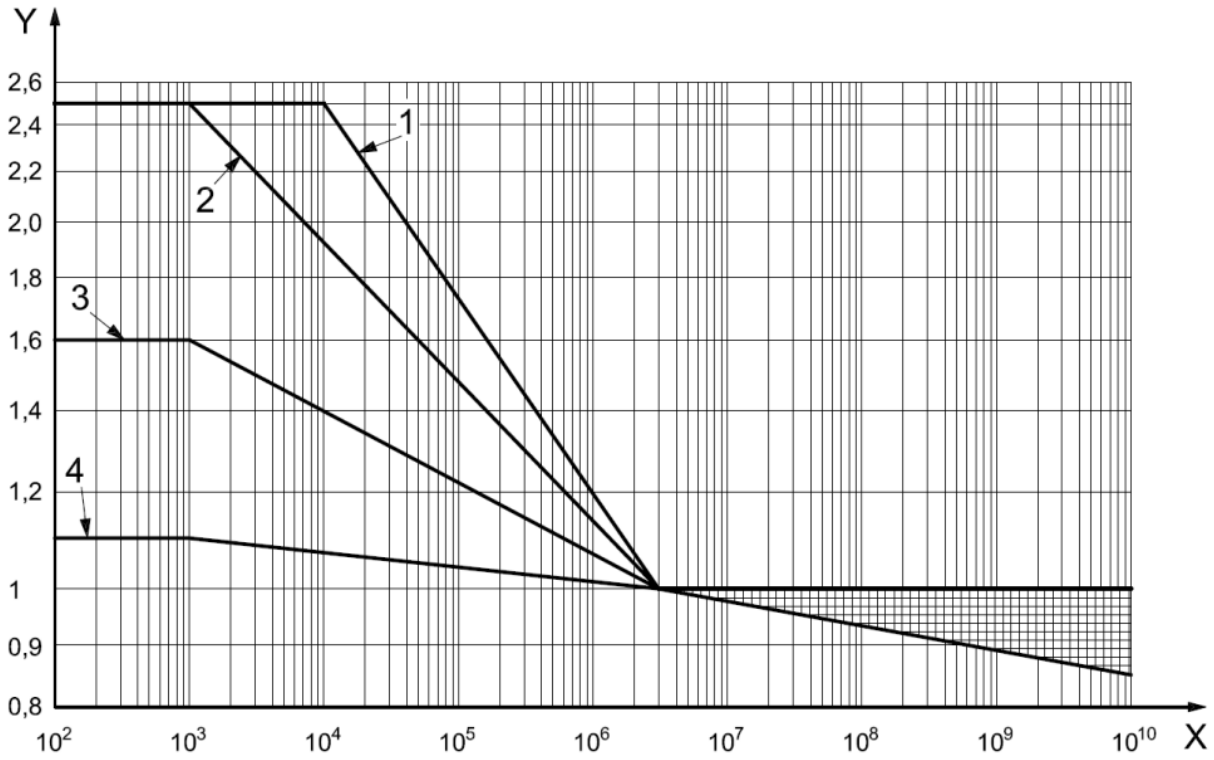

Figure 32. S-N curve for bending from ISO-6336

Seen in figure 32 is the S-N curve for bending, which is taken from ISO-6336:3. The y-axis represents the “life factor”, which is a factor the stresses found from the material data is multiplied.

For the powder metal, the S-N curve and its corresponding material data is found in KissSoft [6], which is a design software for mechanical engineering applications, see table 11 and 12..

Contact	
S [MPa]	cycles
1500	1
1500	2.88e5
1160	1e7
1032	5e7

Table 11. Material data for the S-N curve, contact, PM

Bending	
S [MPa]	cycles
1050	1
1050	1.69e4
700	2.88e5
574	1.16e6

Table 12. Material data for the S-N curve, bending, PM

5.3.1 Adjusted reliability

The S-N curve can be adjusted in order to allow higher loads. This is done by decrease the reliability of the mechanical life. Instead of defining the failure when one percent of the test fails, the definition can be set to an arbitrary number. From Shigley's Mechanical Engineering design [8], the adjustment can be done via dividing the stress levels on the S-N curve with a constant, K_r. This constant is calculated for each reliability, R, as

$$\mathrm{K}_r = \begin{cases} 0.658 - 0.0759\ln(1-R), & 0.5 < R < 0.99 \\ 0.50 - 0.109\ln(1-R), & 0.99 < R < 0.9999 \end{cases} \quad (39)$$

Two reliabilities of interest are 95 and 90 percent. This yields

$$K_{r,95\%} = 0.885$$
$$K_{r,90\%} = 0.833$$

For the case hardened wrought steel, the material data for the adjusted S-N curves are as seen in table 13 and 14 and depicted in figure 33 and 34.

Contact, case hardened wrought steel			
99% reliability	**95% reliability**	**90% reliability**	
S [MPa]	S [MPa]	S [MPa]	cycles
2400	2711	2882	1
2400	2711	2882	1e5
1500	1694	1801	5e7
1275	1440	1531	1e10

Table 13. Material data for contact, case hardened wrought steel

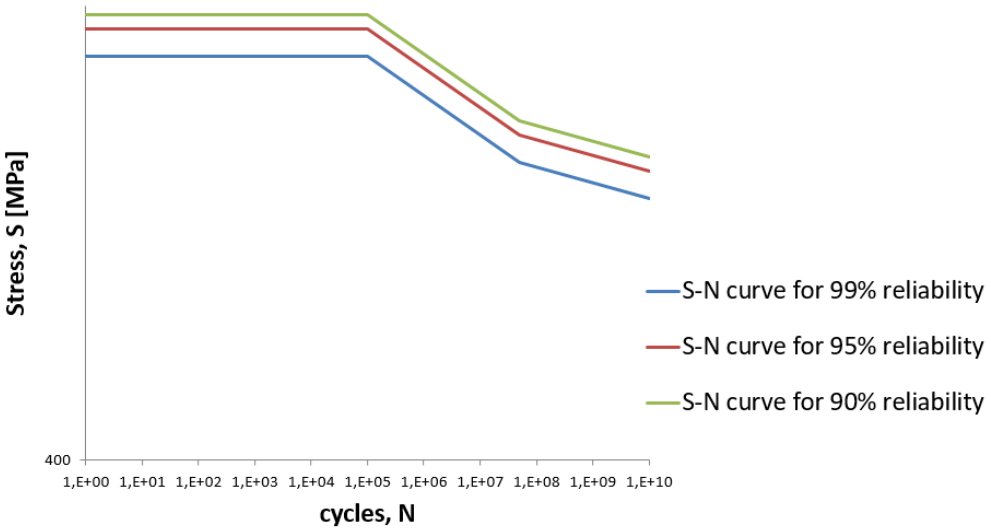

Figure 33. S-N curve for sprockets in contact. Case hardened wrought steel

Bending, case hardened wrought steel			
99% reliability	**95% reliability**	**90% reliability**	
S [MPa]	S [MPa]	S [MPa]	cycles
2300	2598	2762	1
2300	2598	2762	1e3
920	1039	1105	3e6
782	883	939	1e10

Table 14. Material data for bending, case hardened wrought steel

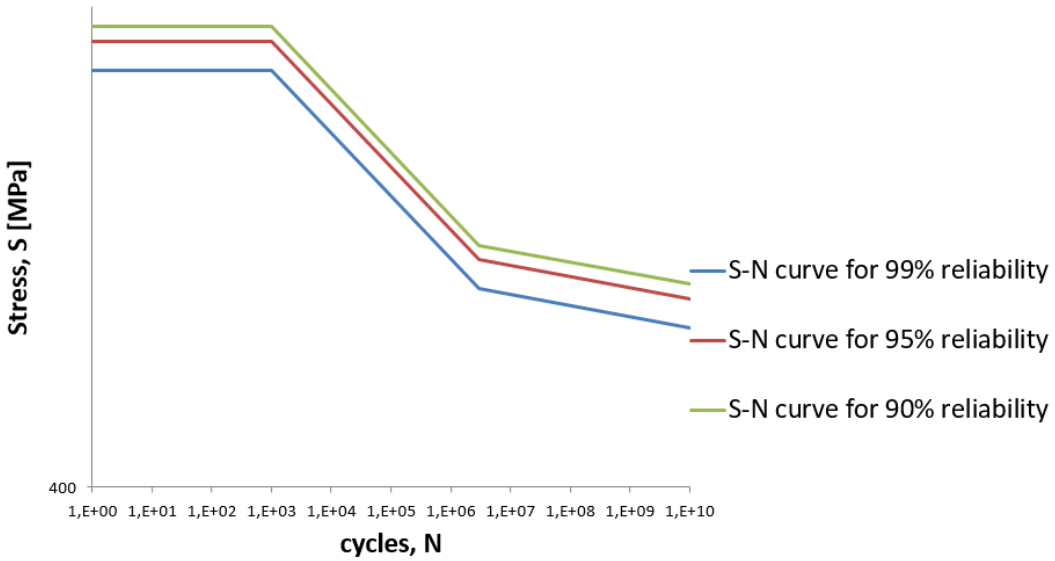

Figure 34. S-N curve for sprockets in bending. Case hardened wrought steel

Seen in table 14 and 15 are material data for PM in the different S-N curves given the reliabilities. Table 14 shows contact and table 15 shows bending.

Contact, PM			
99% reliability	**95% reliability**	**90% reliability**	
S [MPa]	S [MPa]	S [MPa]	cycles
1500	1694	1801	1
1500	1694	1801	2,88e5
1160	1310	1393	1e7
1032	1166	1239	5e7

Table 14. Material data for contact, PM

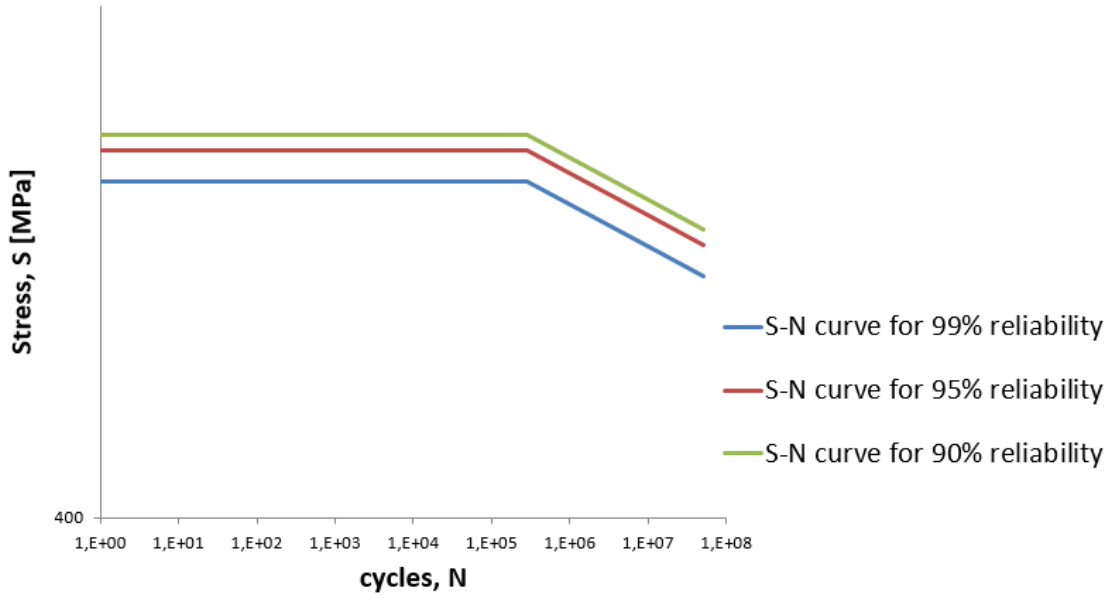

Figure 35. S-N curve for sprockets, contact. Powder metal

Bending, PM			
99% reliability	**95% reliability**	**90% reliability**	
S [MPa]	S [MPa]	S [MPa]	cycles
1050	1186	1261	1
1050	1186	1261	1,69e4
700	791	841	2,88e5
574	648	689	1,16e6

Table 15. Material data for bending, PM.

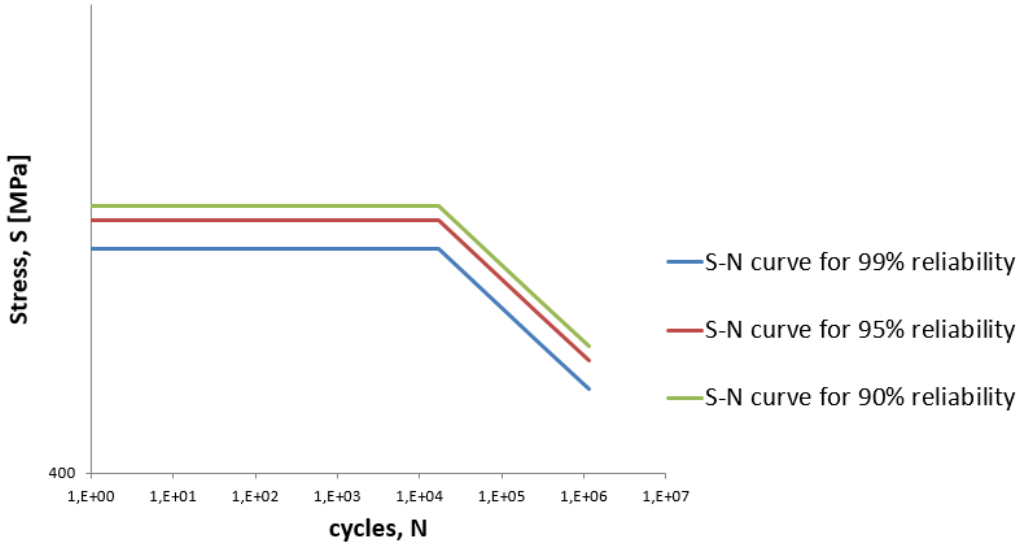

Figure 36. S-N curve for sprockets, bending. Powder metal

5.4 Material data

The material data used are the following

Sprockets

Case hardened wrought steel [6]
E = 210 GPa
v = 0.3

Powder metal [6]
E = 164 GPa
v = 0.28

Links [6]

E = 210 GPa
v = 0.3

5.5 Fatigue result

These results are based on the sprockets. The material is case hardened wrought steels. There are three different results of interest; the total damage, the fatigue safety factor, and the static safety factor.
The total damage is calculated from Palmgren-miner, the fatigue safety factor is defined as the factor between 100% and the result of the total damage, and the static safety factor is defined as the factor between the highest contact pressure / bending stress compared to the highest allowed stress. From figure 9 in ISO 6336-3, the highest allowed stress for bending is 2.5 times higher than the allowed stress, which are seen in the material data in table 14. Equal, for contact, the maximum allowed stress can be seen from figure 6 in ISO 6336-2, which is 1.6 times higher than the allowed stress, seen from table 15.

The result sheets seen in figure 37, 38, 39 and 40 are constructed in Excel. Using the load spectra and calculating the contact force and bending stress for each load, and its corresponding number of cycles, the damage could be calculated. Then, the damage from each load was summed, and the total damage was obtained.

It is desired to have a safety factor for each result, i.e. the result should not be in the close proximity of failure. In this application, the safety factor for static load is set to 1.2 for contact and 1.3 for bending. In the result sheets in figure 37-40, green color denotes the result being on the right side of the safety factor, and red denotes the result being on the wrong side.

Each dot in the S-N curve represent a stress level and its corresponding number of cycles. In figure 39, it can be seen that the stresses in contact when it comes to PM exceeds the maximum allowed stress limit for the 99% reliability. Theoretically, this means that failure will occur. Using the modified S-N curves allows for these stresses.

5.5.1 Result, case hardened wrought steels

Result contact

Used load sharing factor	**30,0**	**%**	**(max tooth load / chain tension)**			
				Drive		**Coast**	
Max contact pressure				1639	Mpa	1464	Mpa
Total damage							
	Reliability			**Drive**		**Coast**	
S-N curve for 99% reliability	99	%		0,0	%	0,0	%
S-N curve for 95% reliability	95	%		0,0	%	0,0	%
S-N curve for 90% reliability	90	%		0,0	%	0,0	%
Fatigue safety factors							
	Reliability			**Drive**		**Coast**	
S-N curve for 99% reliability	99	%		50,0	-	50,0	-
S-N curve for 95% reliability	95	%		50,0	-	50,0	-
S-N curve for 90% reliability	90	%		50,0	-	50,0	-
Static safety factors							
	Reliability			**Drive**		**Coast**	
S-N curve for 99% reliability	99	%		1,46	-	1,64	-
S-N curve for 95% reliability	95	%		1,65	-	1,85	-
S-N curve for 90% reliability	90	%		1,76	-	2,01	-

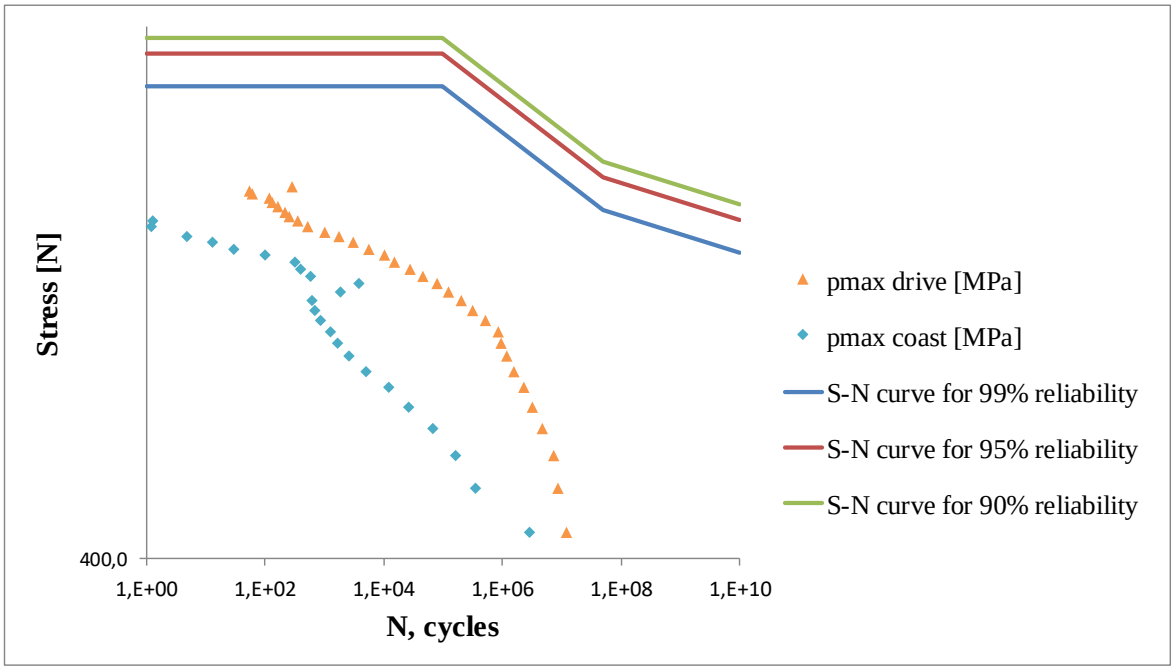

Figure 37. Result for contact fatigue, case hardened wrought steel

Result bending

Used load sharing factor **30,0 %** **(max tooth load / chain tension)**

	Drive		Coast	
Max bending stress	609	Mpa	485	Mpa

Total damage

	Reliability		Drive		Coast	
S-N curve for 99% reliability	99	%	0,0	%	0,0	%
S-N curve for 95% reliability	95	%	0,0	%	0,0	%
S-N curve for 90% reliability	90	%	0,0	%	0,0	%

Fatigue safety factors

	Reliability		Drive		Coast	
S-N curve for 99% reliability	99	%	50,0	-	50,0	-
S-N curve for 95% reliability	95	%	50,0	-	50,0	-
S-N curve for 90% reliability	90	%	50,0	-	50,0	-

Static safety factors

	Reliability		Drive		Coast	
S-N curve for 99% reliability	99	%	3,78	-	4,74	-
S-N curve for 95% reliability	95	%	4,27	-	5,35	-
S-N curve for 90% reliability	90	%	4,54	-	5,69	-

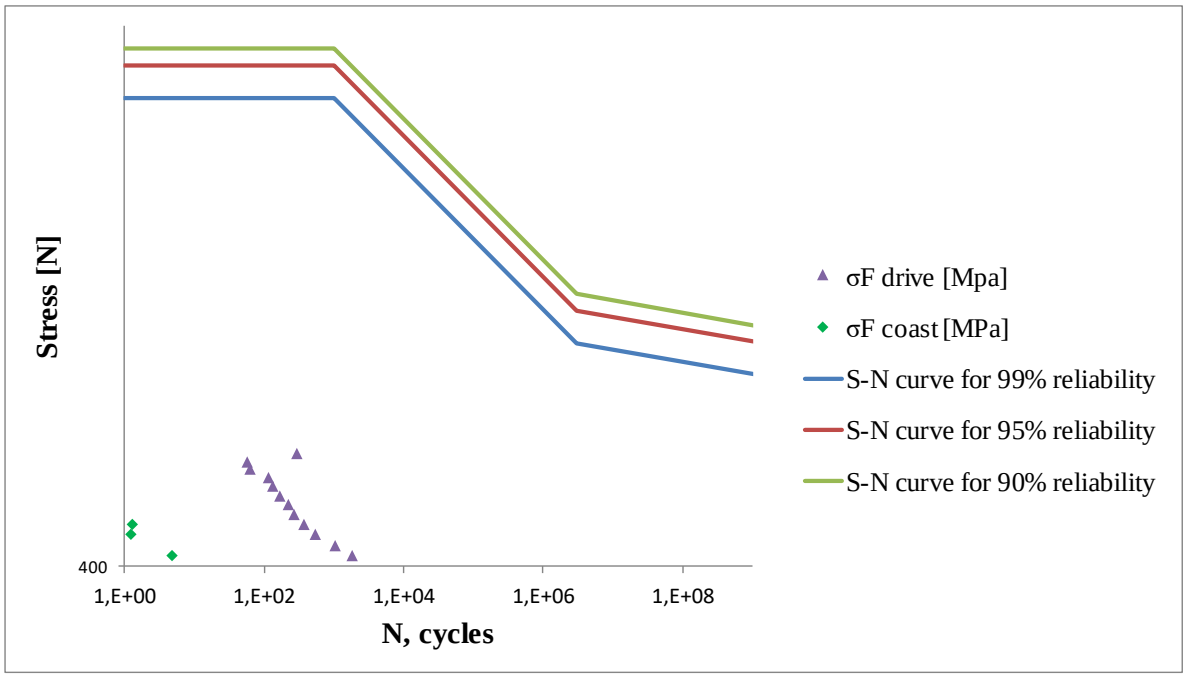

Figure 38. Result for bending fatigue, case hardened wrought steel

5.5.2 Result, powder metallurgy

Result contact

Used load sharing factor **30,0 %** **(max tooth load / chain tension)**

	Drive		Coast	
Max contact pressure	1592	Mpa	1422	Mpa

Total damage

	Reliability		Drive		Coast	
S-N curve for 99% reliability	99	%	4,7	%	0,0	%
S-N curve for 95% reliability	95	%	1,0	%	0,0	%
S-N curve for 90% reliability	90	%	0,4	%	0,0	%

Fatigue safety factors

	Reliability		Drive		Coast	
S-N curve for 99% reliability	99	%	21,1	-	50,0	-
S-N curve for 95% reliability	95	%	50,0	-	50,0	-
S-N curve for 90% reliability	90	%	50,0	-	50,0	-

Static safety factors

	Reliability		Drive		Coast	
S-N curve for 99% reliability	99	%	0,94	-	1,06	-
S-N curve for 95% reliability	95	%	1,06	-	1,19	-
S-N curve for 90% reliability	90	%	1,13	-	1,29	-

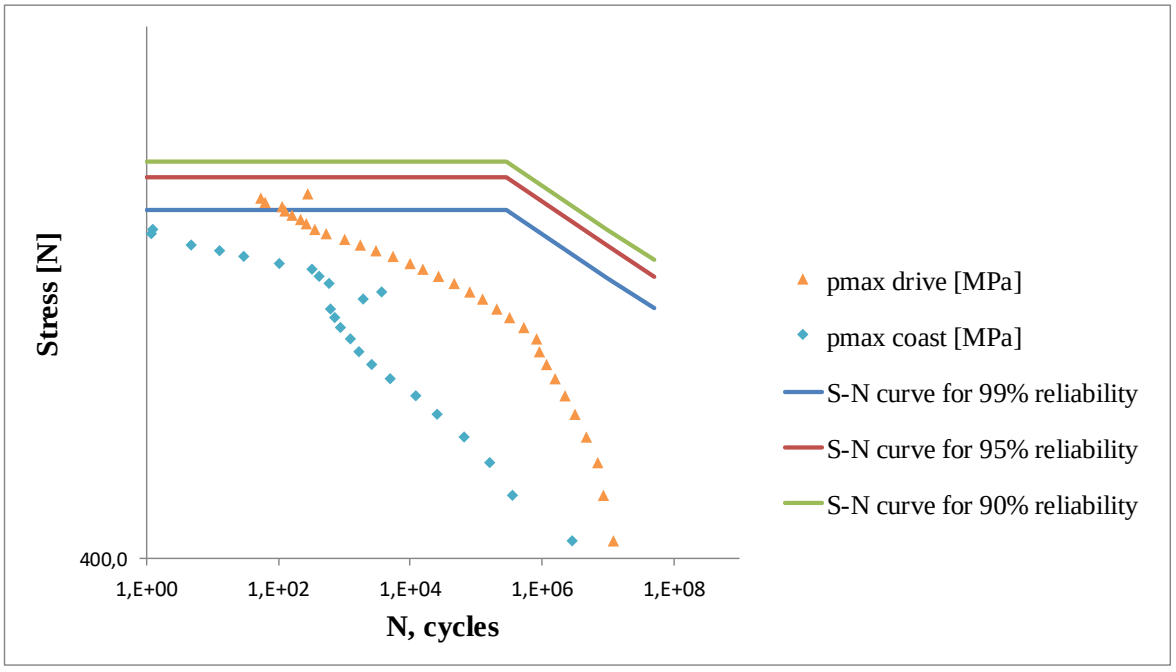

Figure 39. Result for contact fatigue, PM

Result bending

Used load sharing factor **30,0 %** **(max tooth load / chain tension)**

	Drive		Coast	
Max bending stress	609	Mpa	485	Mpa

Total damage

	Reliability		Drive		Coast	
S-N curve for 99% reliability	99	%	0,8	%	0,0	%
S-N curve for 95% reliability	95	%	0,3	%	0,0	%
S-N curve for 90% reliability	90	%	0,2	%	0,0	%

Fatigue safety factors

	Reliability		Drive		Coast	
S-N curve for 99% reliability	99	%	50,0	-	50,0	-
S-N curve for 95% reliability	95	%	50,0	-	50,0	-
S-N curve for 90% reliability	90	%	50,0	-	50,0	-

Static safety factors

	Reliability		Drive		Coast	
S-N curve for 99% reliability	99	%	1,72	-	2,16	-
S-N curve for 95% reliability	95	%	1,95	-	2,44	-
S-N curve for 90% reliability	90	%	2,07	-	2,60	-

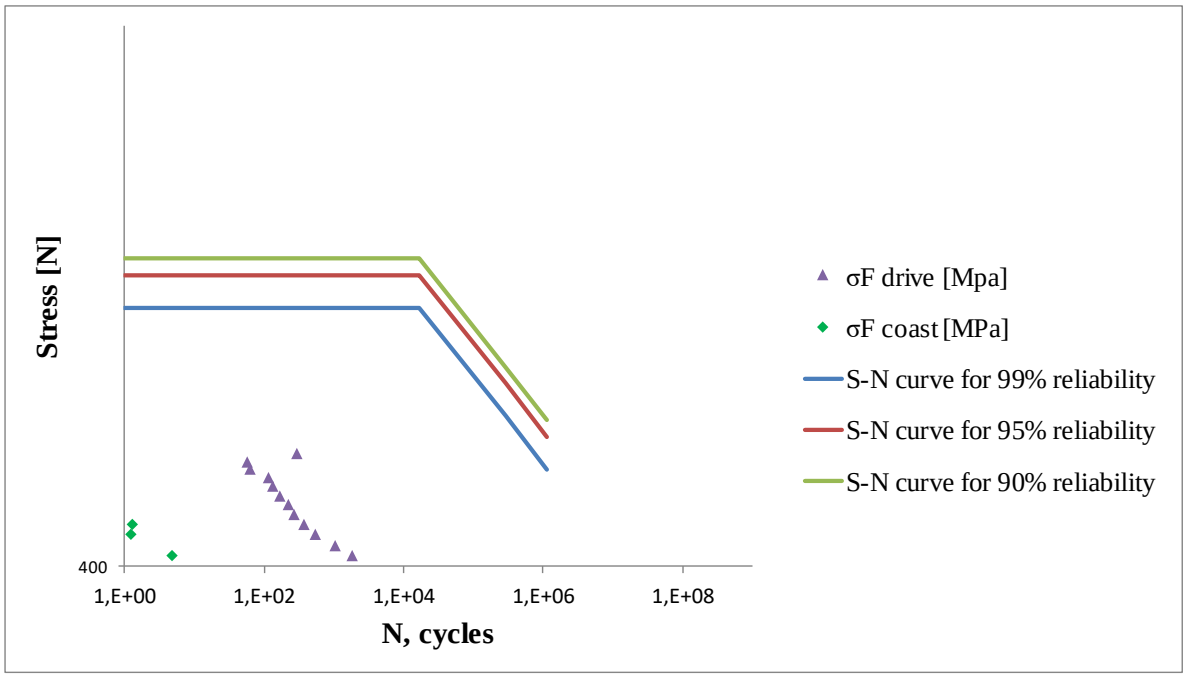

Figure 40. Result for bending fatigue, PM

6. Discussion

In this report, the dynamic loads on a Hy-Vo chain sprocket have been calculated. Based on these loads, a fatigue calculation was made with different materials. The results from the fatigue calculation shows that the design of the sprockets employed today is unnecessary conservative. The total damage on the teeth, both in contact and bending, is close to 0.0% which shows that there are some elbow room for lowering the costs by changing the manufacturing method to something cheaper, which might also lower the expected life.

6.1 Contact pressure

The most interesting part of the result of the fatigue calculation comes from the contact pressure in the powder metal sprocket. This shows that problems should be expected if this was used instead of the case hardened wrought steel used today. In order to overcome these problems, there are different ways of approach. The most sensible should be to reinforce the surface of the teeth in some way. This can be done by using heavy force to raise the density locally on the surface. This would leave the sprocket with a better capability of handling greater forces on its teeth. Seen in figure 41 is this contact damage in a real case test. It is called piano teeth due to its appearance where the area with contact damage is darker than the undamaged area. For more pictures, see appendix 1.

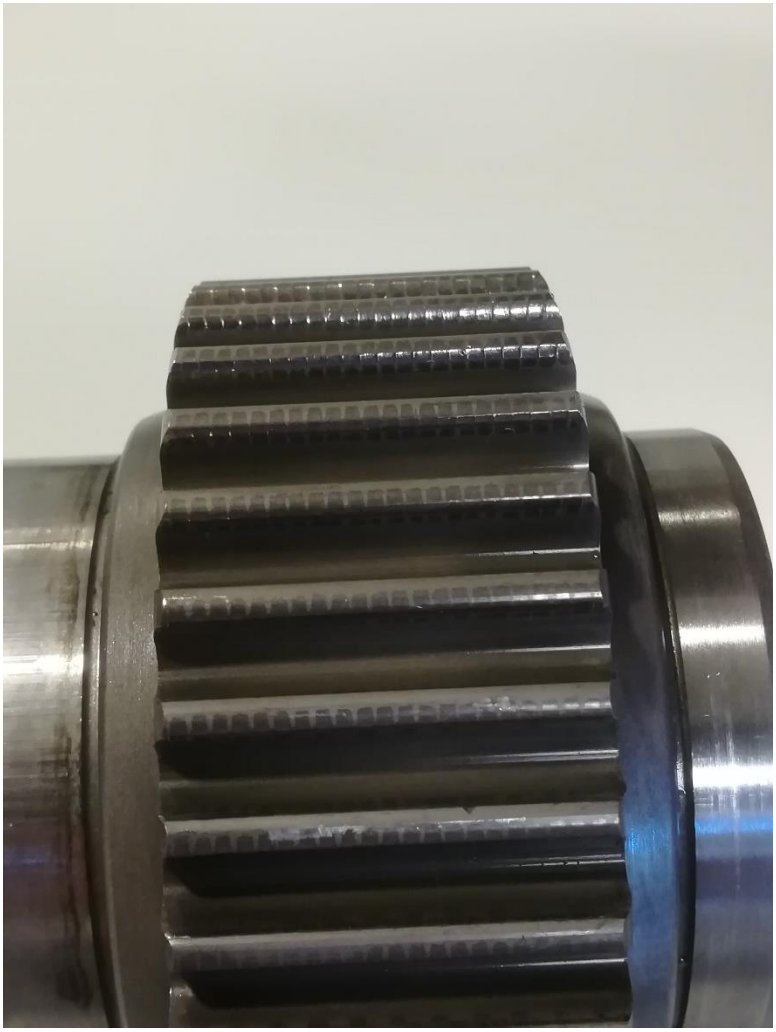

Figure 41. Piano teeth, arising from fatigue

6.2 Sources of error

Several different sources of error related to the execution of this thesis can be identified. The first and most obvious is the approximative design of the sprocket in the ADAMS simulation. The simulation uses a standard silent chain with round pins, unlike the Hy-Vo chain which uses rocker-pins. Reducing the degrees of freedom might change the load distribution in one way or the other. Furthermore, the design of both the sprockets and the chain is an approximation of the reality, and the real profiles might have a different load distribution. However, the parameters which is of greatest importance, intuitive, is the number of teeth in engagement and the pitch diameter. These parameters are the same in both the real design as in the approximated, which make it more likely to be fairly accurate. The major changes lies within the top and bottom radius. But since these parameters does not affect the contact between the sprockets and the chain, it should not induce any major errors.
The simulation in itself also poses as an potential source of error. Since it is only a model of reality, it cannot be taken as an absolute veracity. Also, the simulation setting are based on recommendations, and the simulation output was not always smooth when the program had problem converging the calculations. This meant that the reading of the result had to take place at an estimated point, seen as the mean value.

Given this, the simulation is most likely to provide a result with an error within a few percent. The load distribution was changing with the rotational speed and torque input, and by using the highest recorded load distribution and rounding upwards, the margin of safety should be good enough.

The potential sources of error in the geometry section are fewer. One of the more likely is the determination of where the root of the tooth is located. There was several different ways of conducting this, but the procedure described in ISO-6336 was used. The calculation of the stresses in the root using the FEM should be very accurate and should not pose as a potential error.

7. Conclusion

This thesis shows that the sprockets employed today are produced with an unnecessary conservative approach. The method of manufacturing is relatively expensive and has room for improvement. One of the more competitive change is going to powder metal as a material and powder metallurgy as manufacturing method. This would cut the costs and result in a greater profit for the company.

The problems concerning this transition is related to the loads which the teeth experience. The bending stresses would not pose as an issue, but the contact pressure would. The main issue are the highest peaks of torque where high contact pressure arises. This would induce pitting in the teeth with destroyed surfaces as a consequence.

This might not pose as an issue depending on how this would be handled. If a tooth would snap off due to high load, the sprocket will fail as a whole, but when pitting is induced in the teeth, the sprockets can still operate. There are techniques to harden the surface even further, which would improve the performance.

8. Recommendations and future work

Recommended for BorgWarner is to further evaluate the possibility of changing the manufacturing method to PM. This report shows great possibilities for doing so and given the potential savings in manufacturing, it will most likely be profitable for BorgWarner. Prototypes should be developed and evaluated both in a laboratory and in a real environment.

For future work, the validation of the load distribution should be one of the major concerns. Also, the real profile with the Hy-Vo chain should be implemented in a simulation and compared to the estimated profile. Furthermore, the different approaches for defining the root of the teeth could be investigated in order to make comparisons with the one defined in ISO-6336.
The noise of the transmission when changing to powder metal has not been investigated and with a strive towards more quiet cars and trucks, this should also be investigated.

References

[1] *Number of BorgWarner employees from FY 2009 to FY 2017.* 2017. https://www.statista.com/statistics/381004/number-of-employees-of-borgwarner/ (2018-05-28)

[2] *POLYGONAL EFFECT IN CHAIN DRIVES.* 2012. http://nptel.ac.in/courses/116102012/32. (2018-05-28)

[3] Vedmar, Lars. 2013. *Transmissioner*. 3rd edition.

[4] ISO 6336. *Calculation of load capacity of spur and helical gears*.3rd edition. 2016.

[5] Zhu, Xiaoyin. 2012. *Tutorial on Hertz contact stress*.

[6] KISSsoft is a registered trademark by KISSsoft AG

[7] Suresh, S. *Fatigue of materials.* 2012. 2nd edition. Cambridge: Cambridge University Press

[8] Budynas, Richard G., Nisbett, J. Keith. 2011. *Shigley's Mechanical Engeneering design*. 9th edition. New York: McGraw-Hill Companies Inc.

Appendix 1 – Related pictures

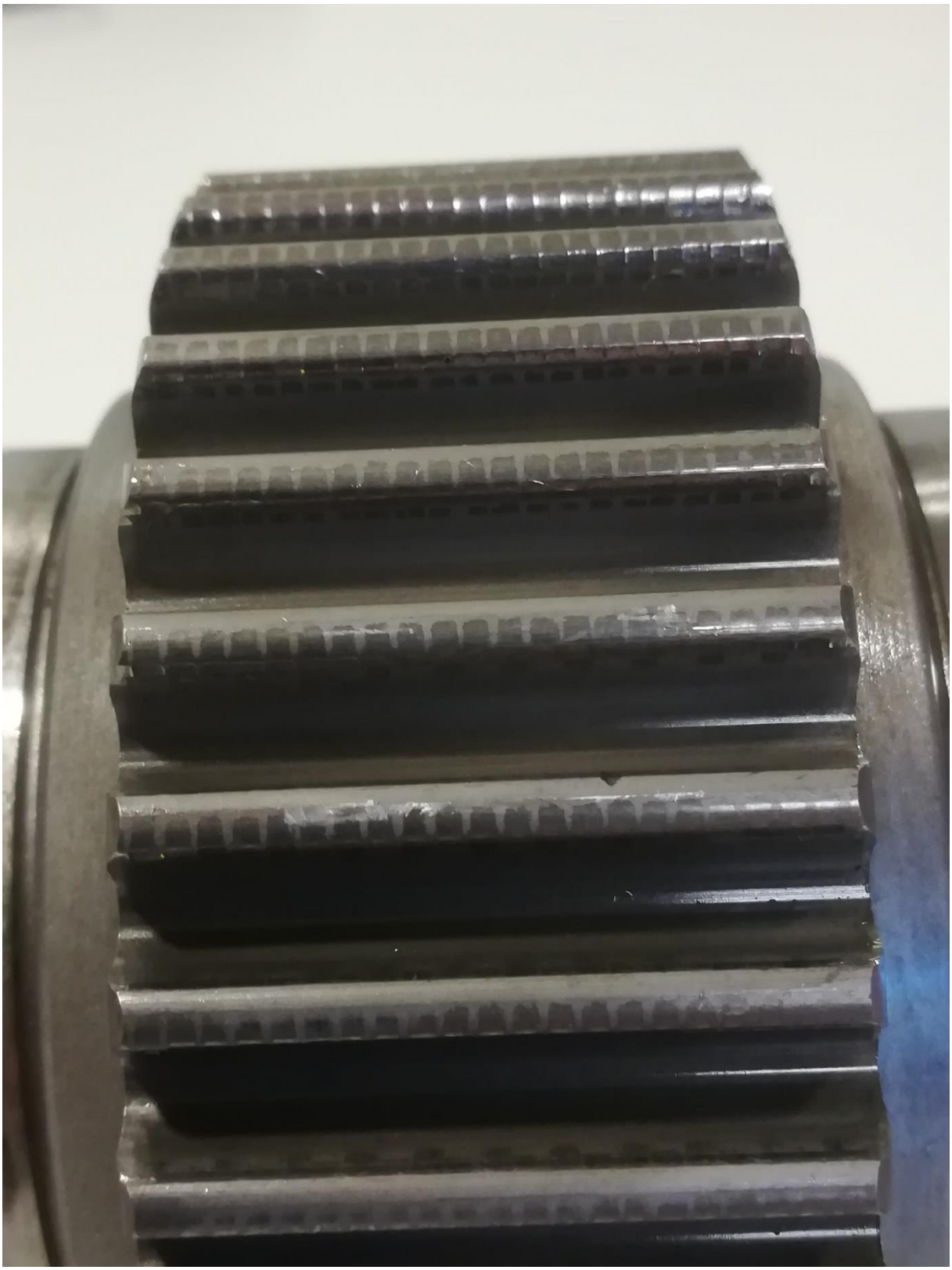

Figur 42. Sprocket with contact fatigue

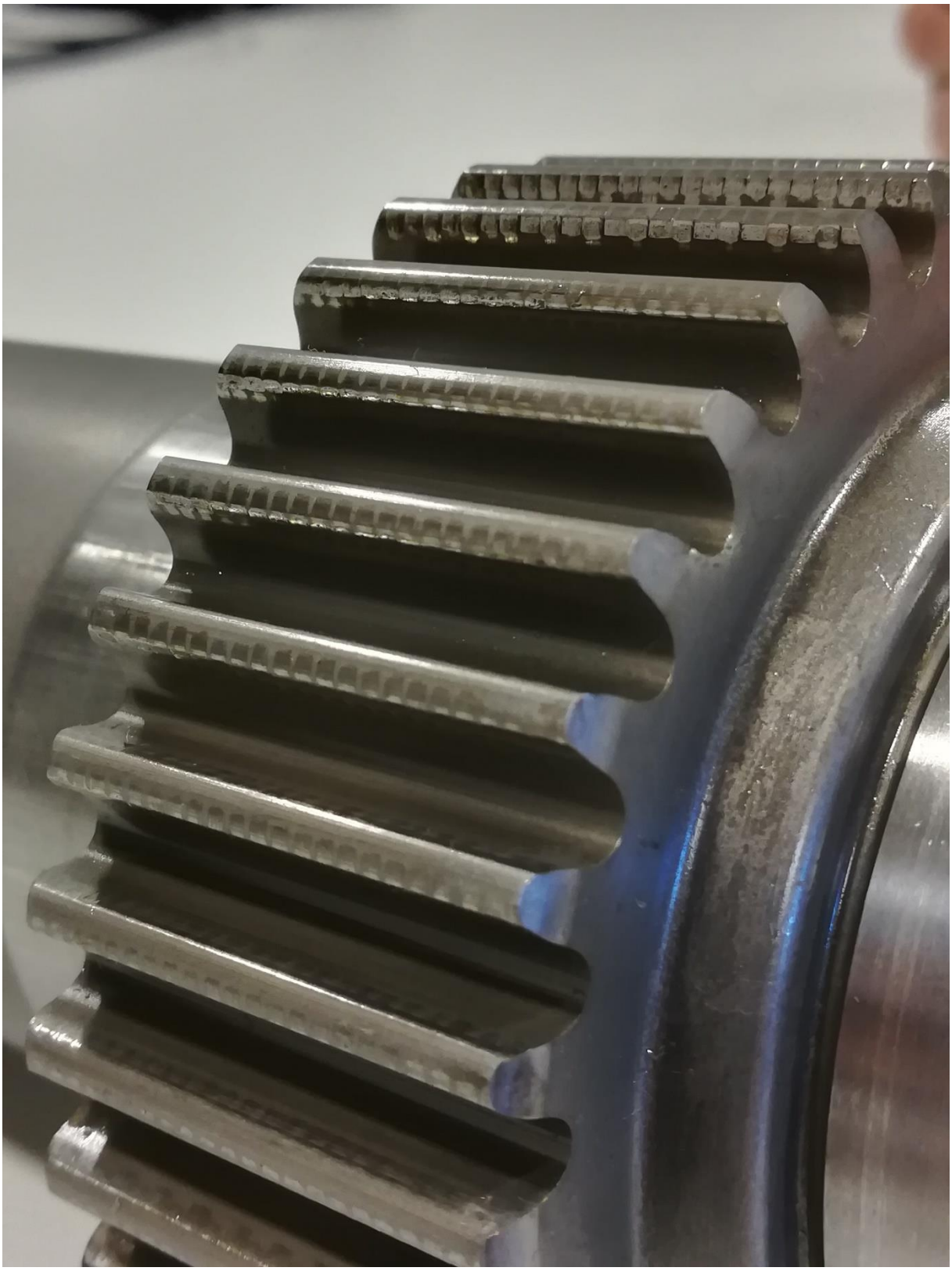

Figure 43. Sprocket with contact fatigue seen from the side

Appendix 2 – Simulations in ADAMS

Note: The units on the x-axis from here on is time, measured in seconds.

500 rpm – 500 Nm

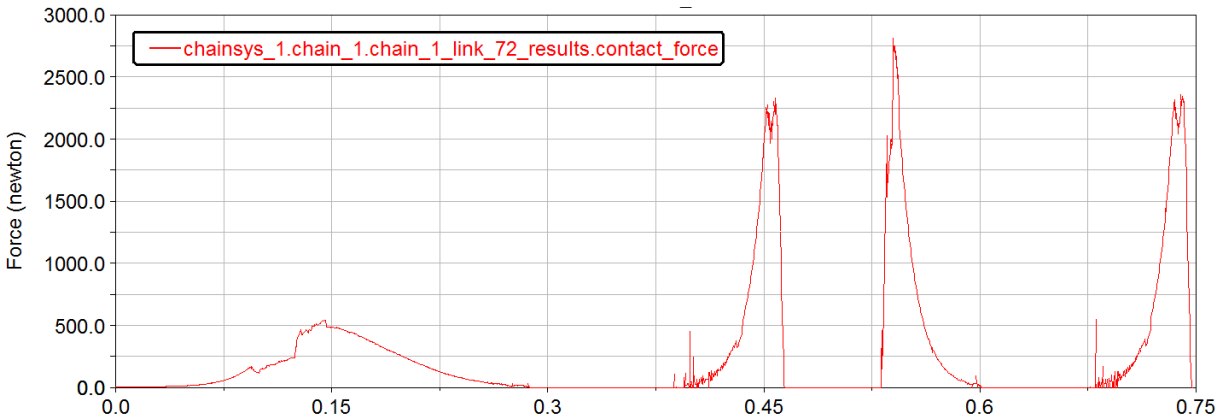

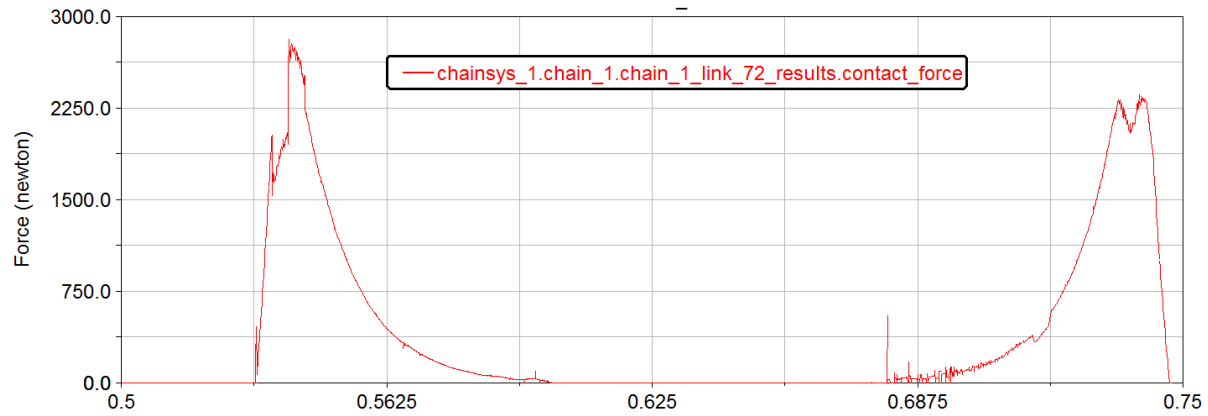

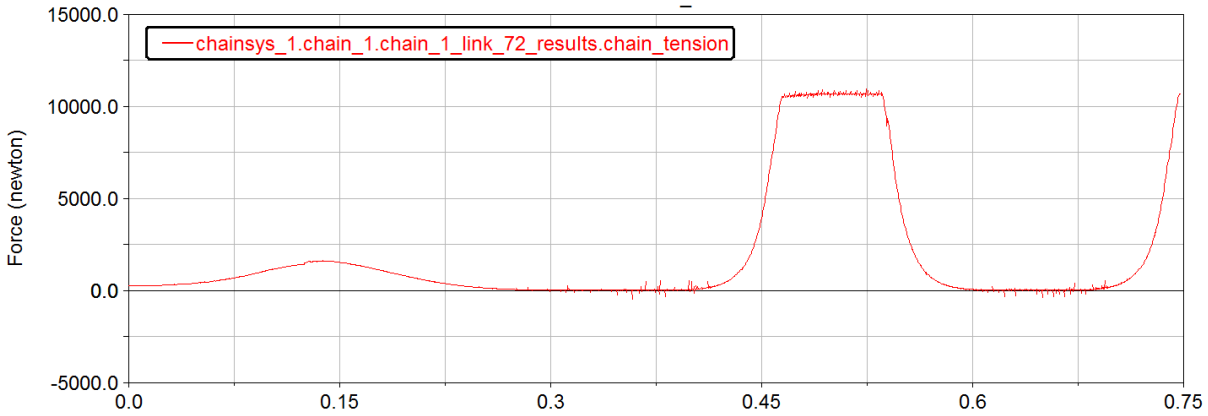

MAX CHAIN TENSION 10882N

MAX CONTACT FORCE 2815N

25.87%

500rpm – 1000Nm

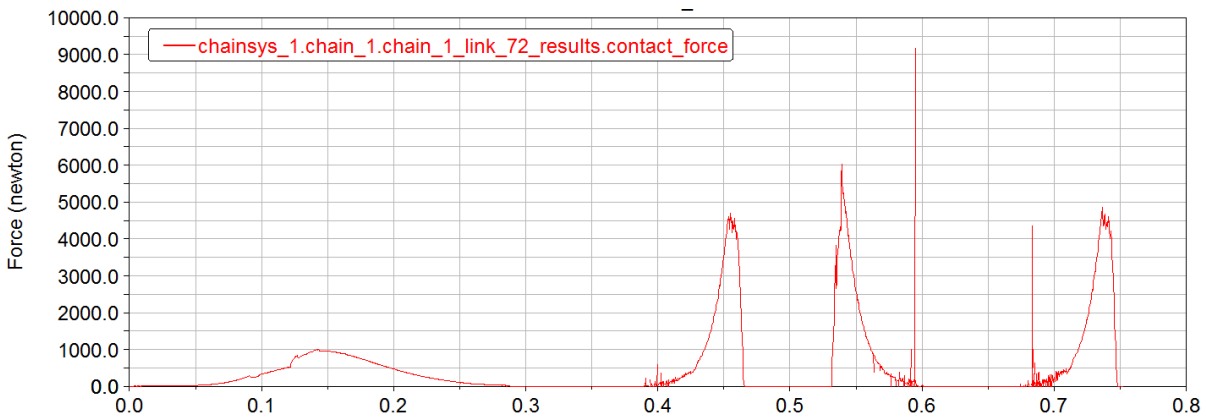

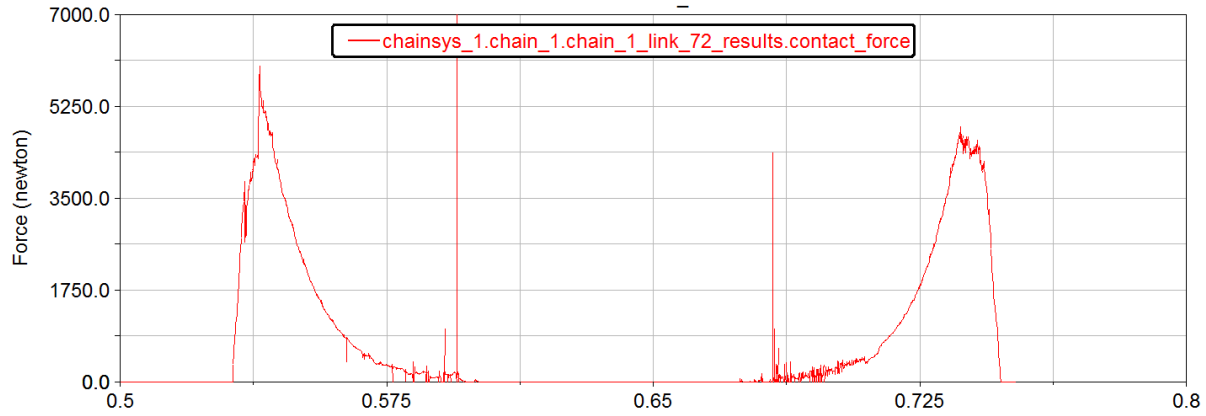

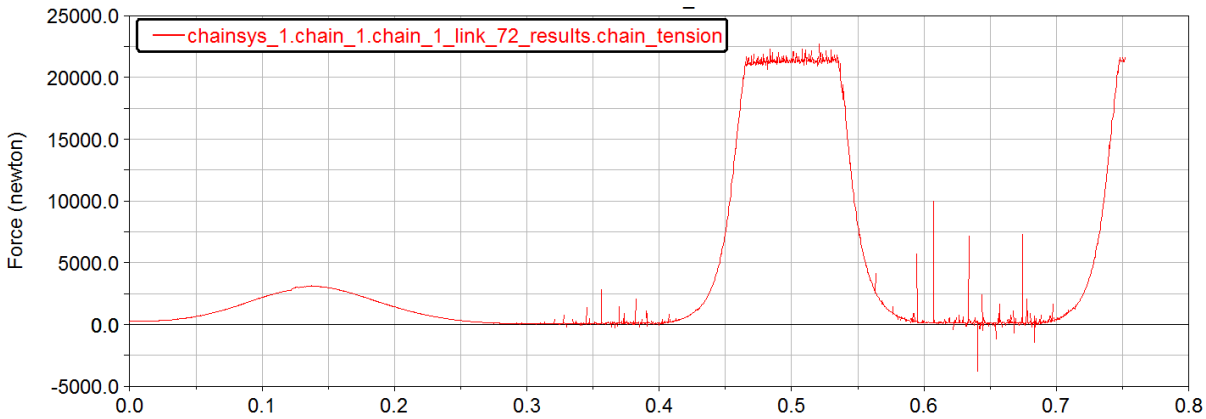

MAX CHAIN TENSION 21850N

MAX CONTACT FORCE 6021N

27.56%

500rpm – 1500Nm

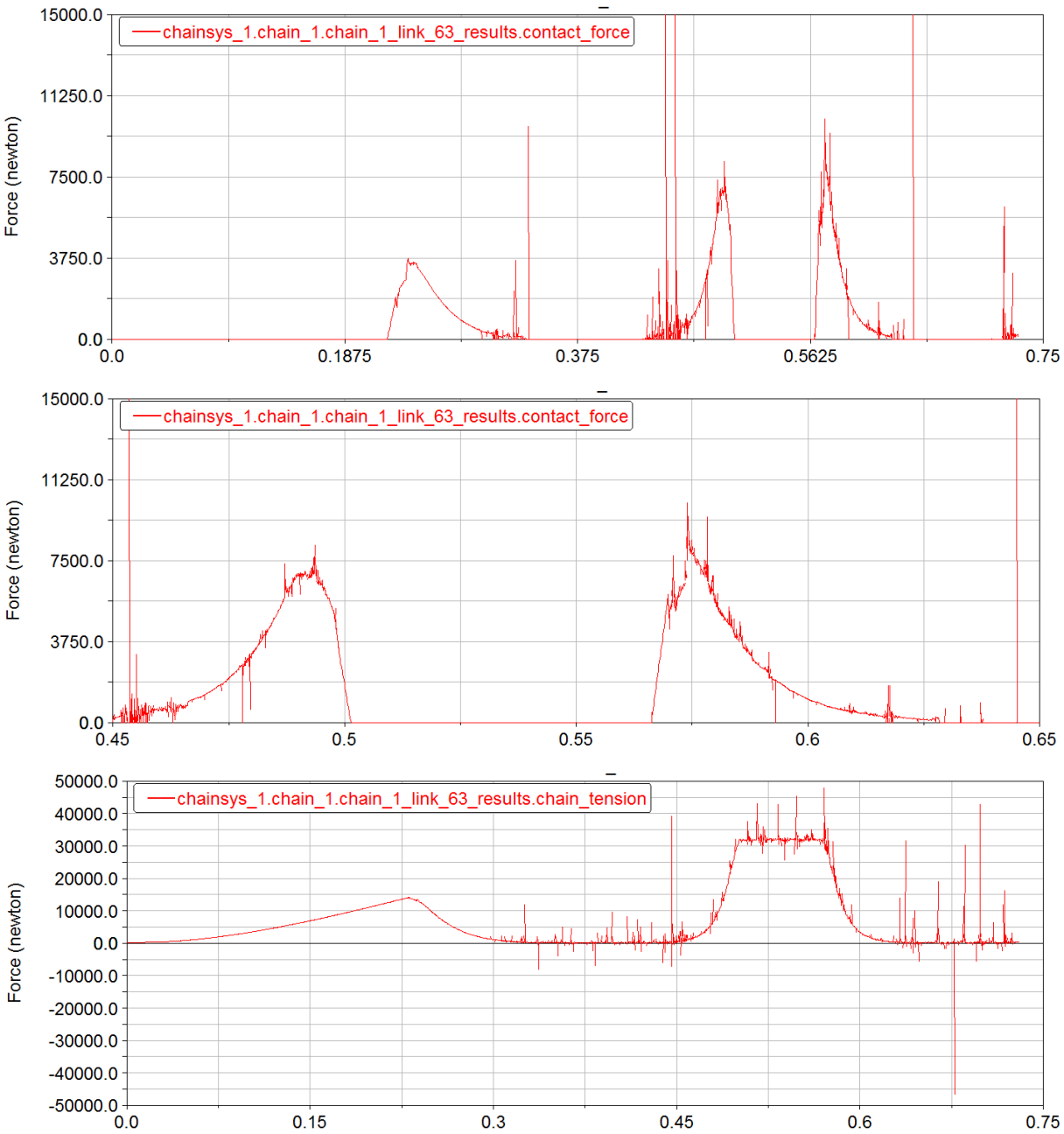

MAX CHAIN TENSION 32400N

MAX CONTACT FORCE 9455N

29.18%

1000 rpm – 500nm

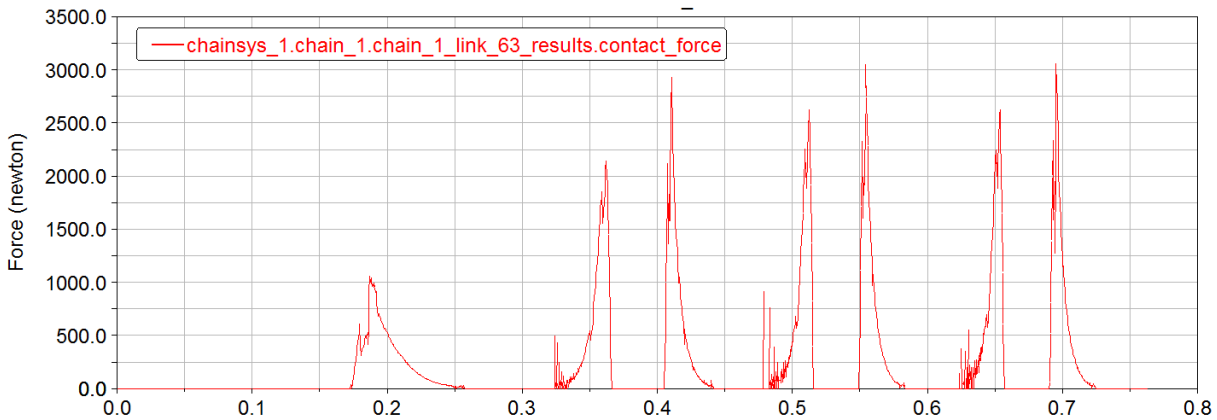

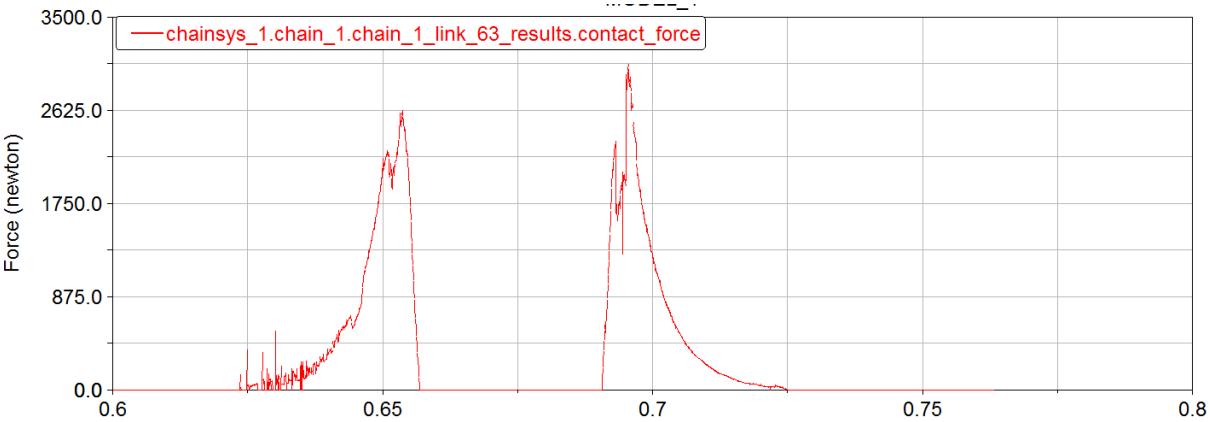

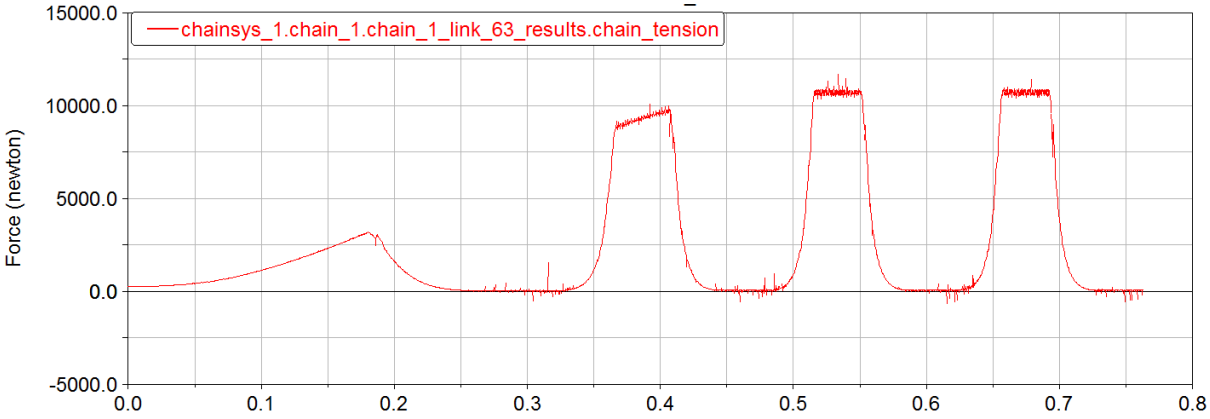

MAX CHAIN TENSION 10900N

MAX CONTACT FORCE 3060N

28.07%

1000 rpm – 1000 Nm

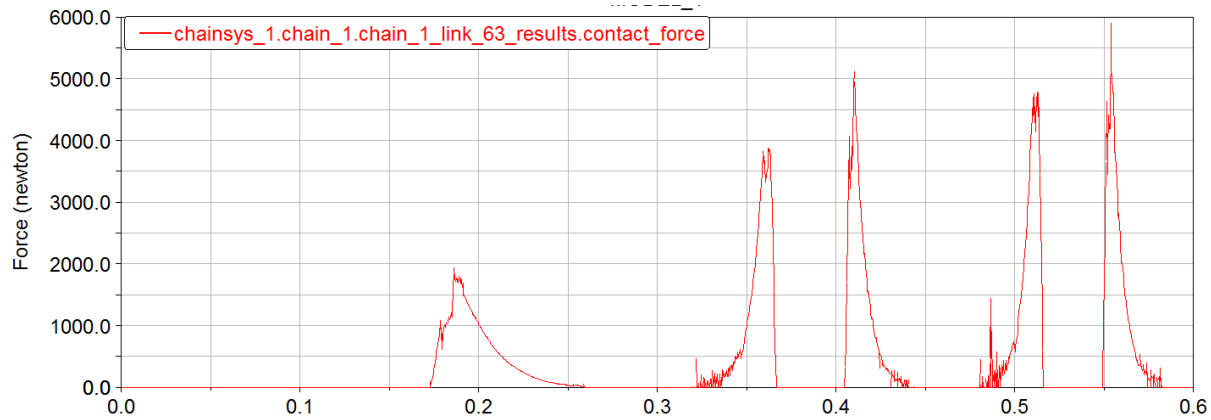

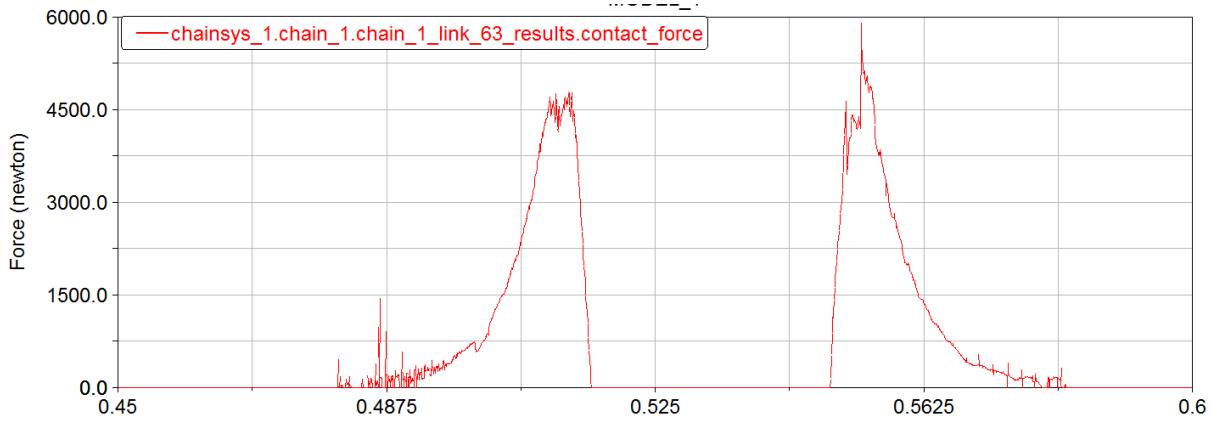

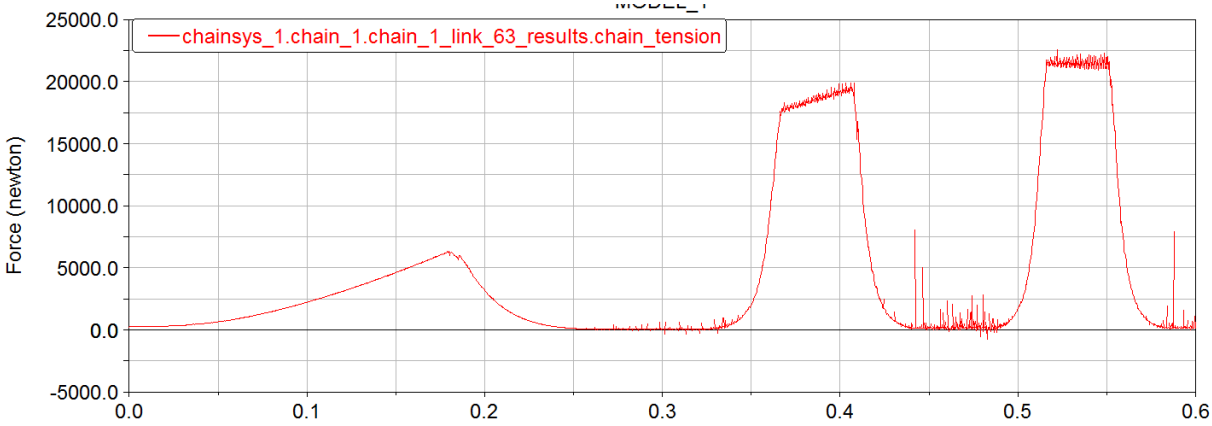

MAX CHAIN TENSION 21920N

MAX CONTACT FORCE 5320N

24.27%

1000 rpm – 1500 Nm

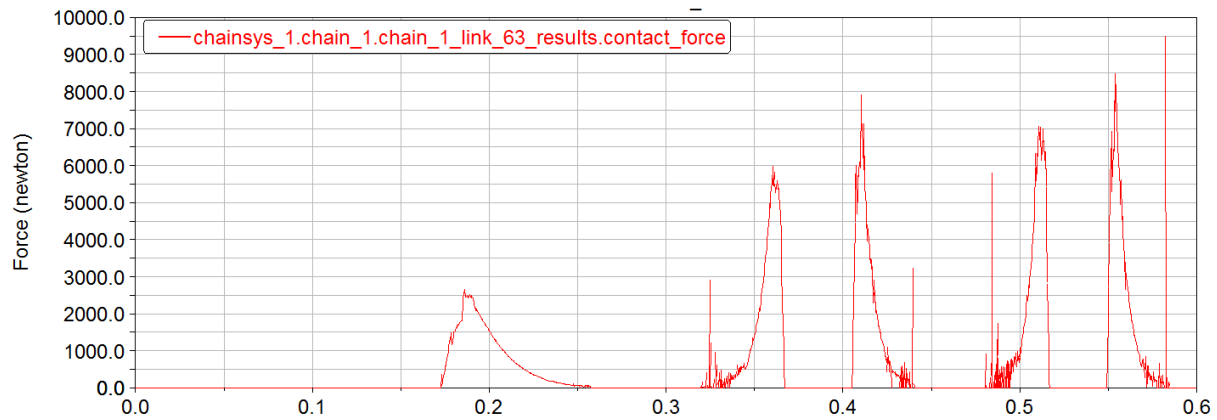

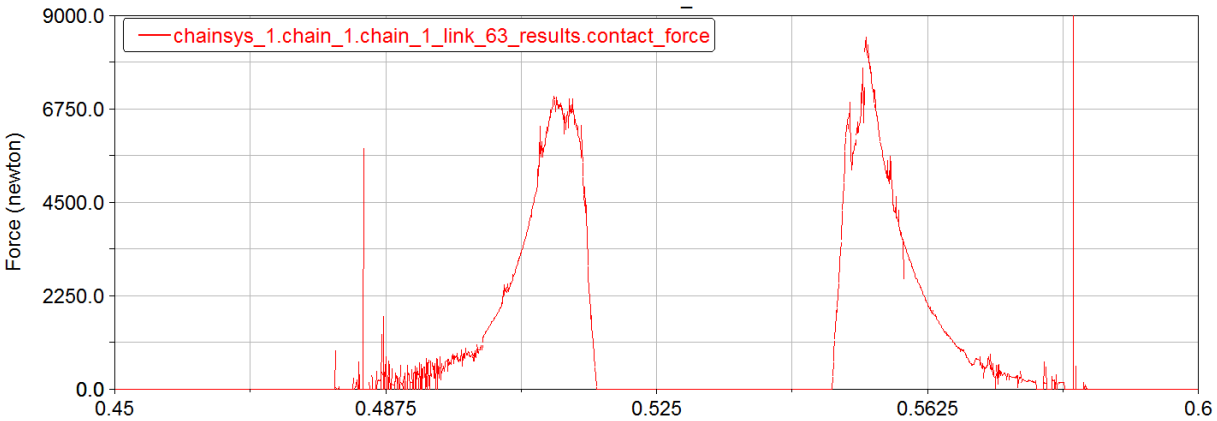

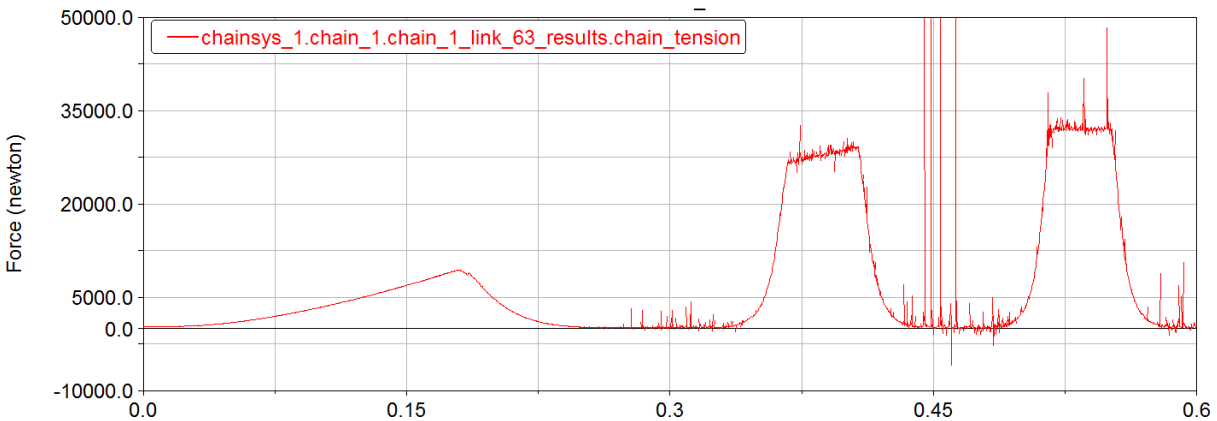

MAX CHAIN TENSION 33600N

MAX CONTACT FORCE 8480N

25.24%

1500 rpm – 500 Nm

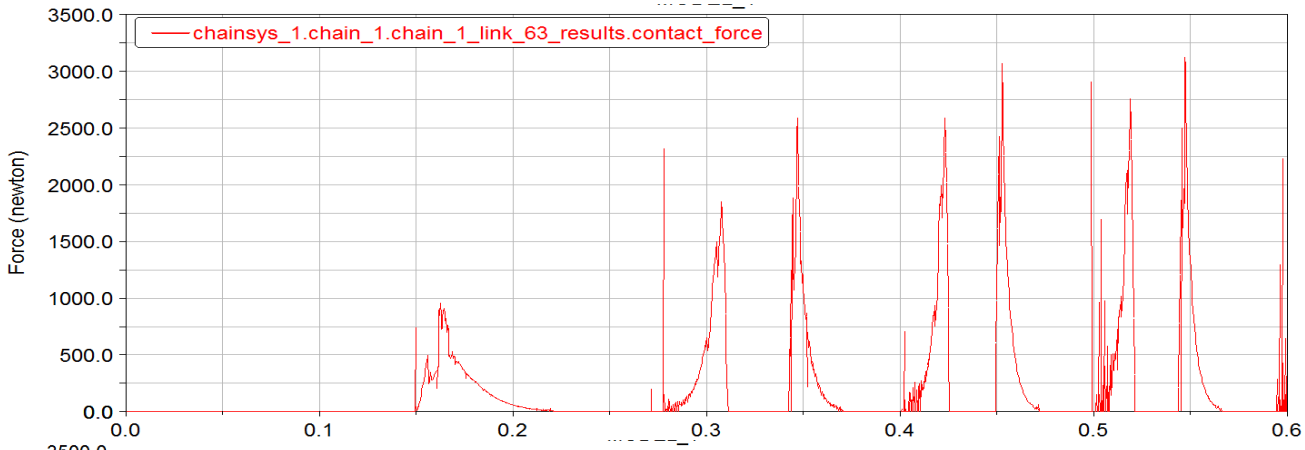

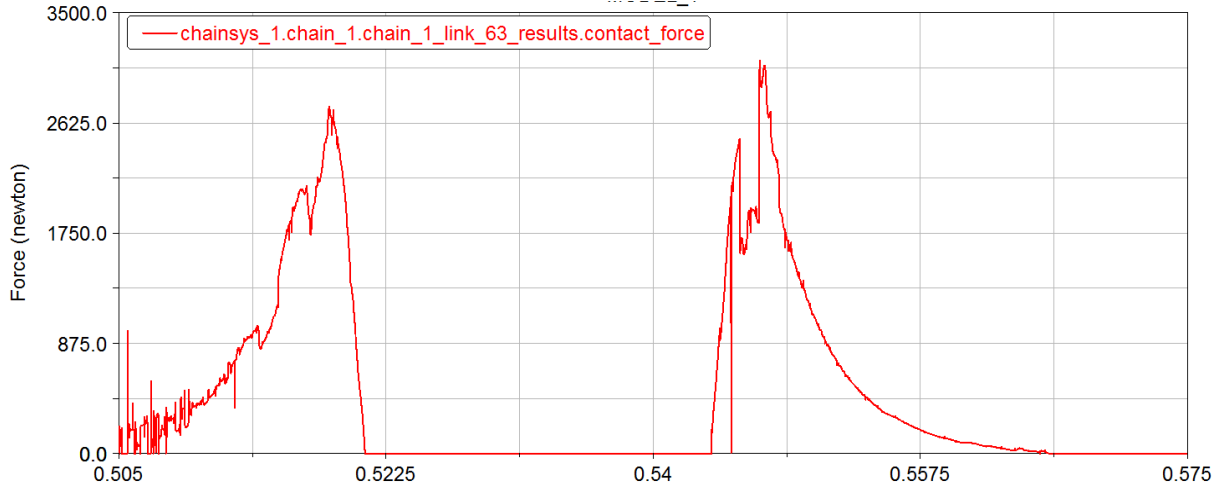

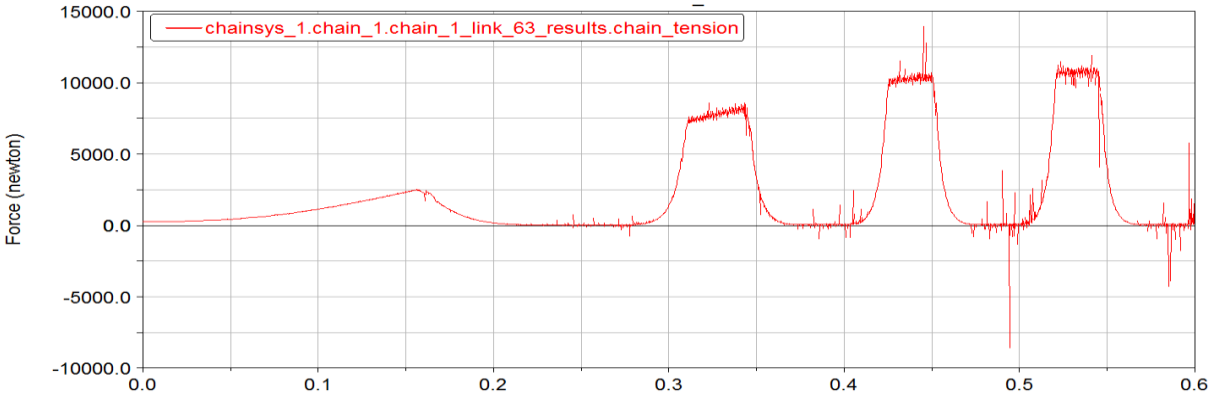

MAX CHAIN TENSION 11120N

MAX CONTACT FORCE 3120N

28.06%

1500 rpm – 1000 Nm

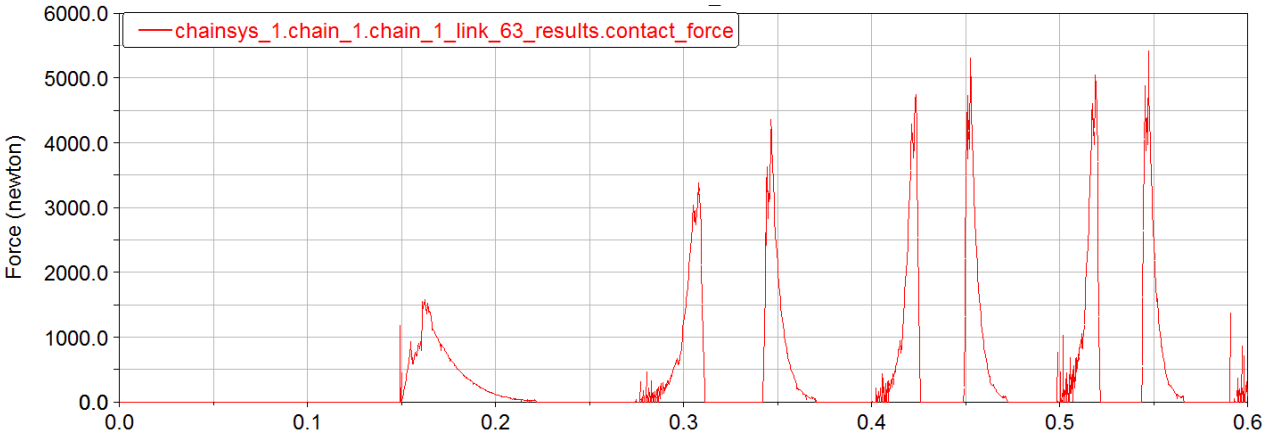

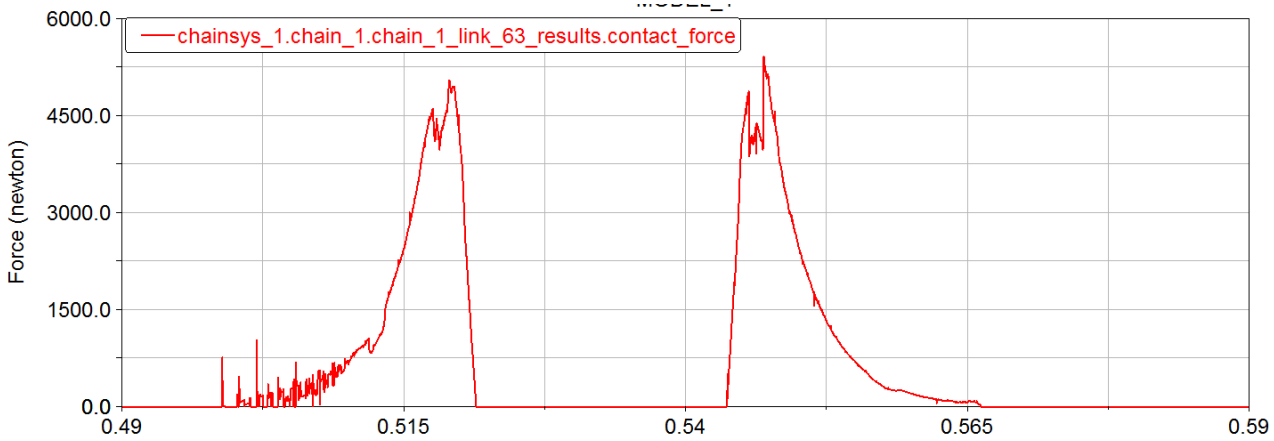

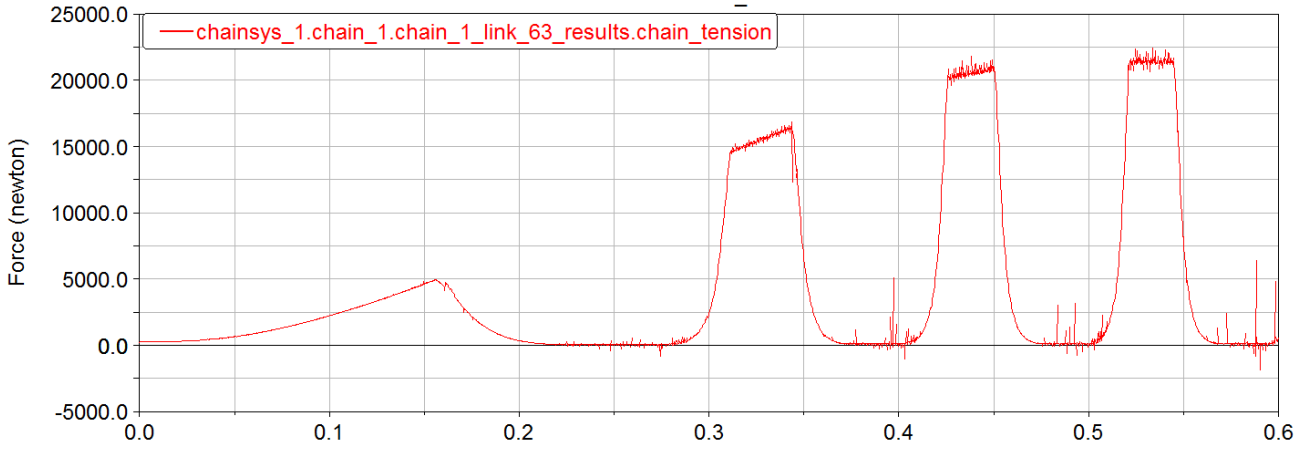

MAX CHAIN TENSION 22010N

MAX CONTACT FORCE 5420N

24.63%

1500 rpm – 1500 Nm

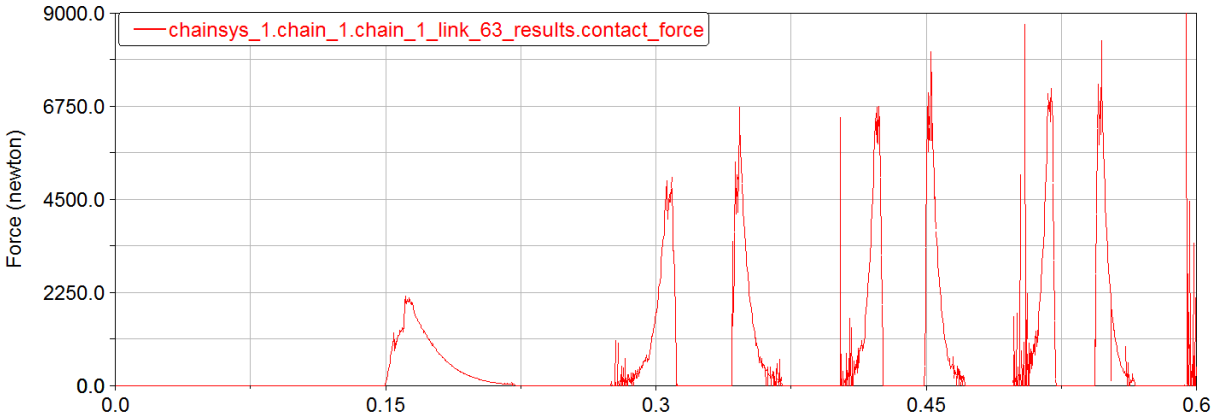

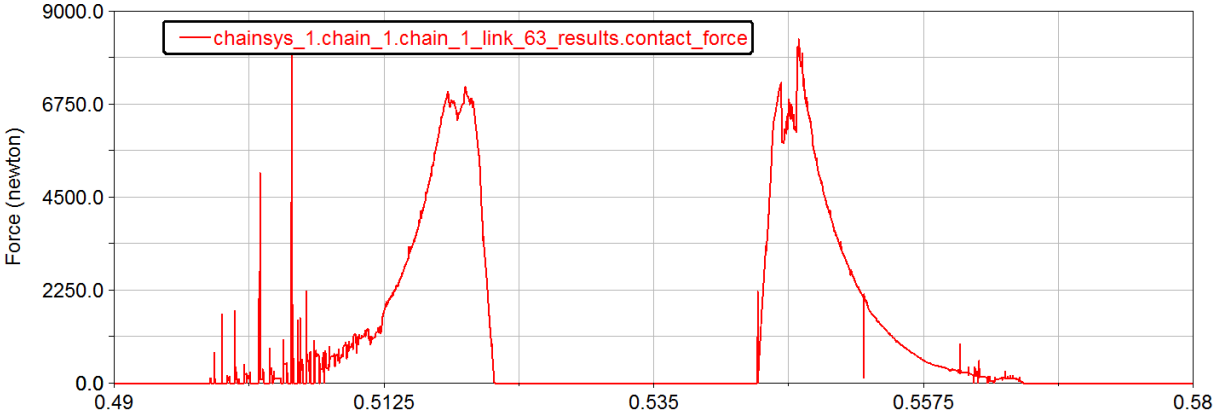

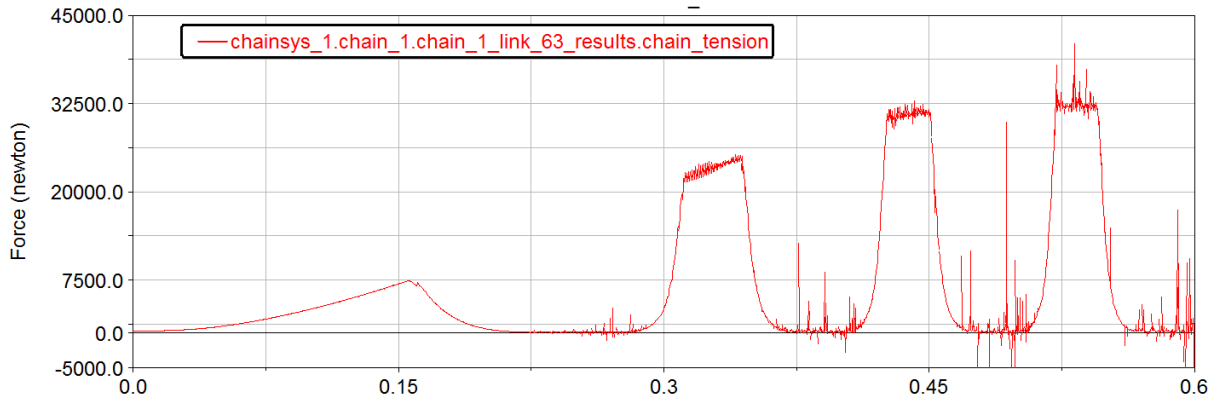

MAX CHAIN TENSION 32600N

MAX CONTACT FORCE 8330N

25.55%

500 rpm – 500 Nm – 0.1% extension

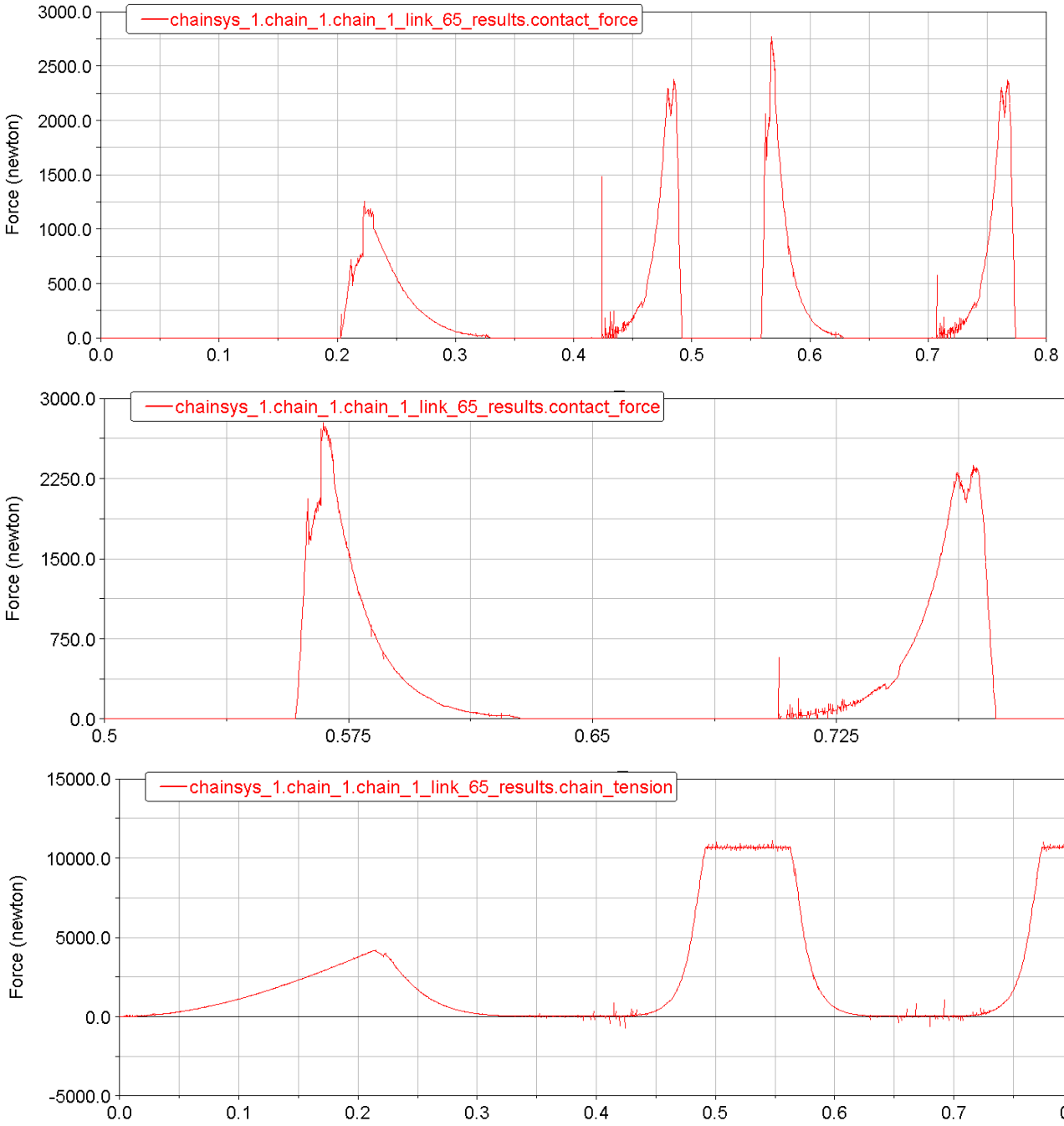

MAX CHAIN TENSION 11110N

MAX CONTACT FORCE 2770N

24.93%

500 rpm – 500 Nm – 0.2% extension

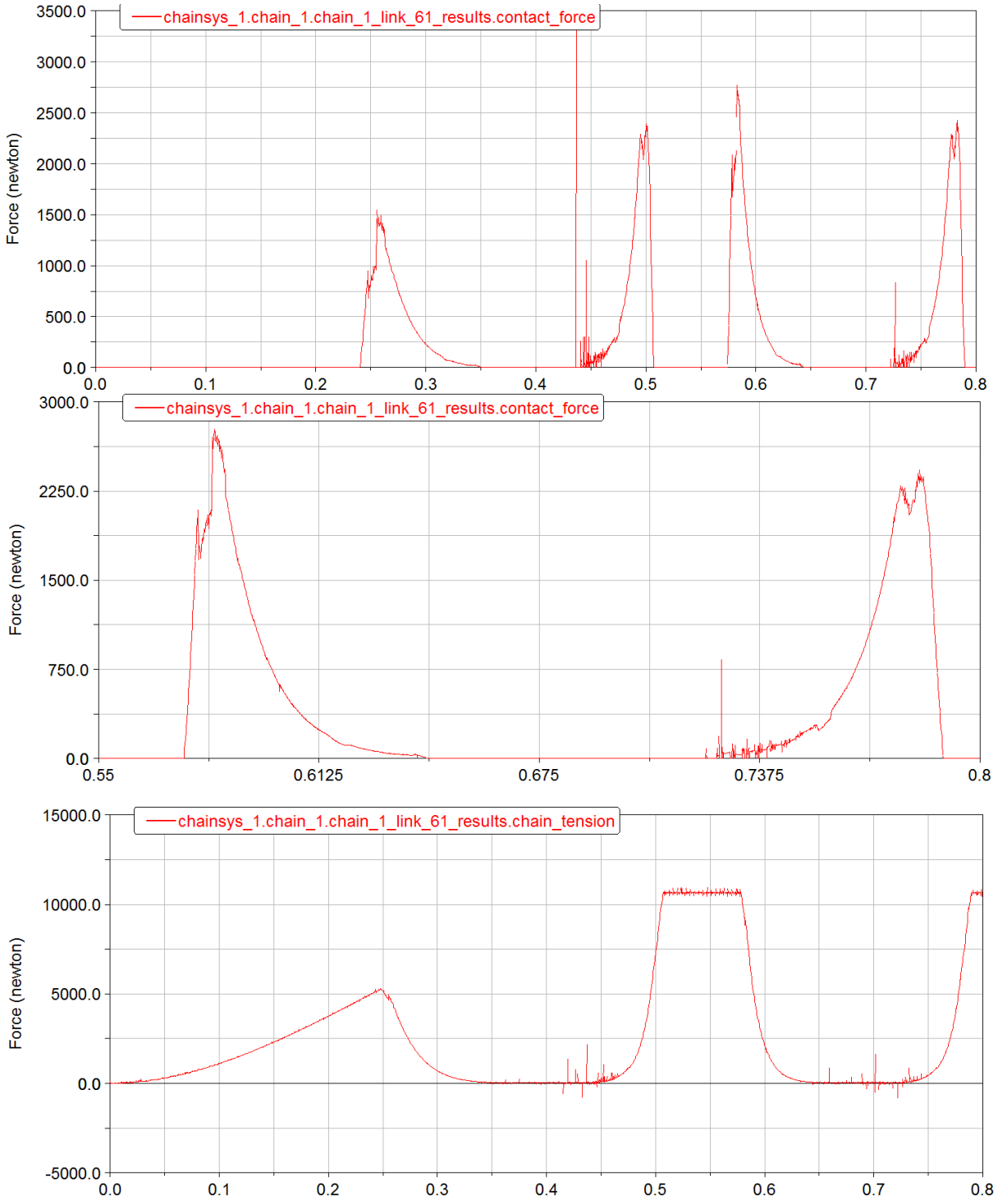

MAX CHAIN TENSION 10850N

MAX CONTACT FORCE 2770N

25.53%

500 rpm – 1500 Nm – 0.1% extension

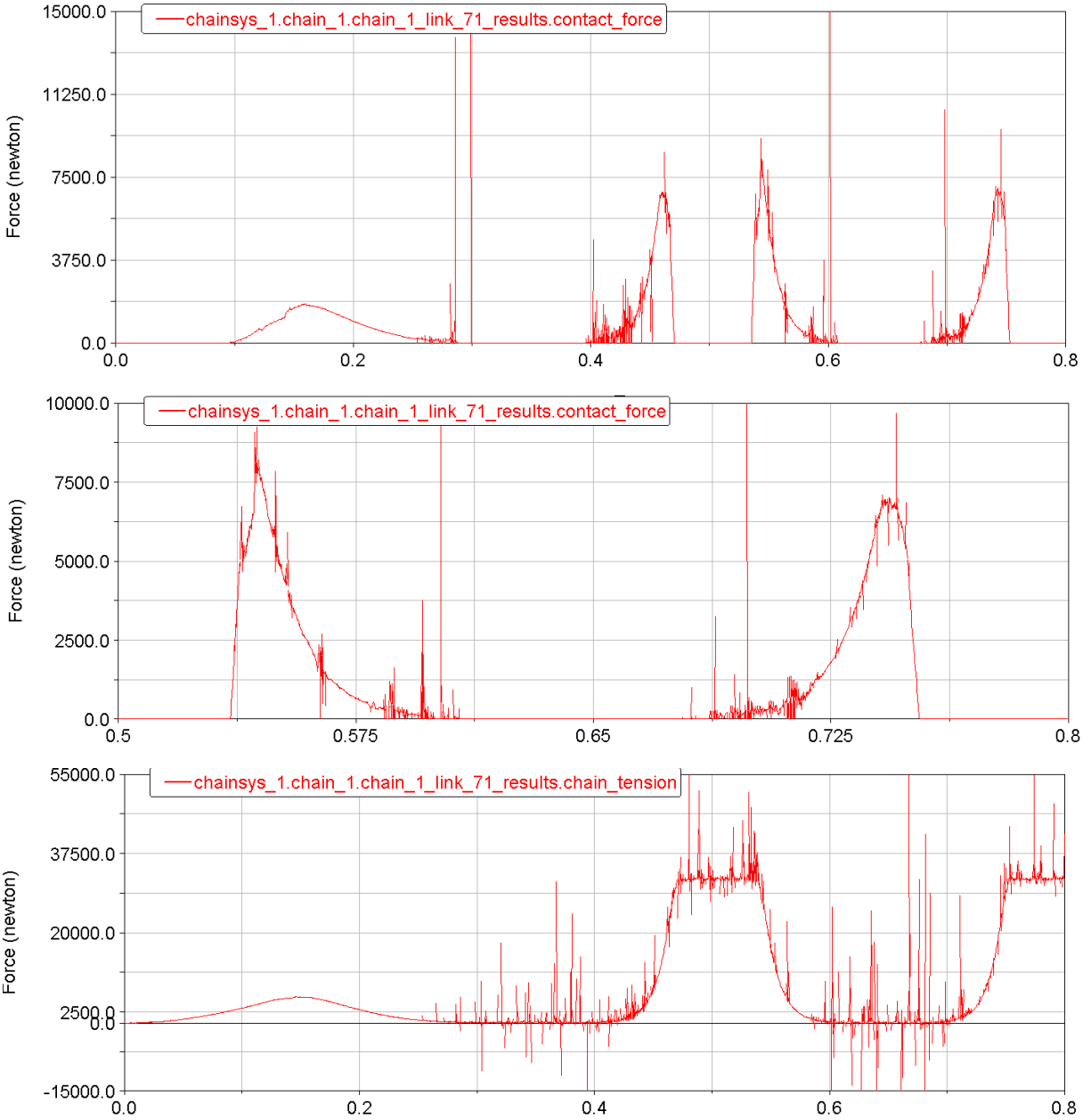

MAX CHAIN TENSION 32200N

MAX CONTACT FORCE 8360N

25.96%

500 rpm – 1500 Nm – 0.2% extension

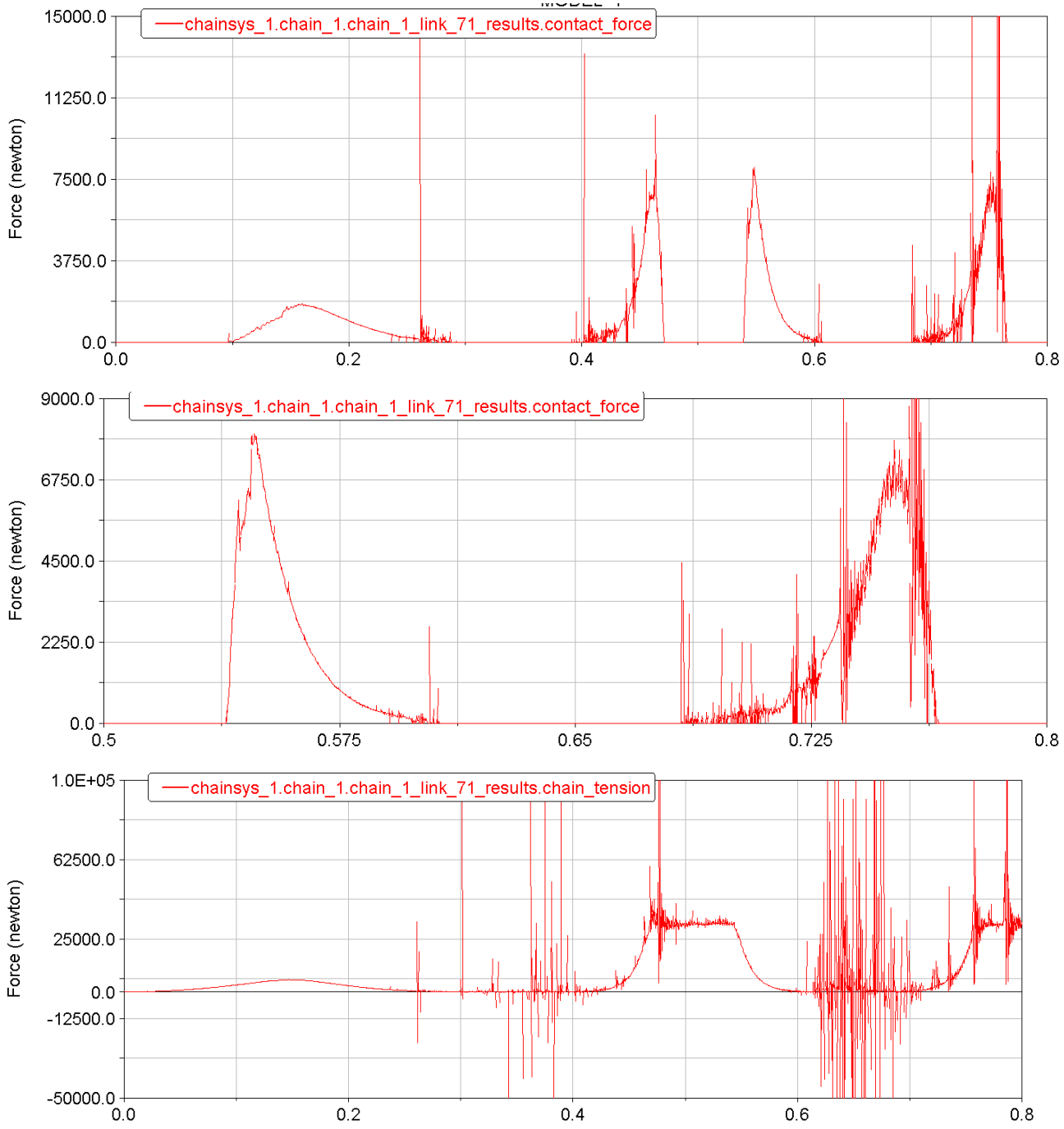

MAX CHAIN TENSION 32200N

MAX CONTACT FORCE 8030N

24.94%

1500 rpm – 500 Nm – 0.1% extension

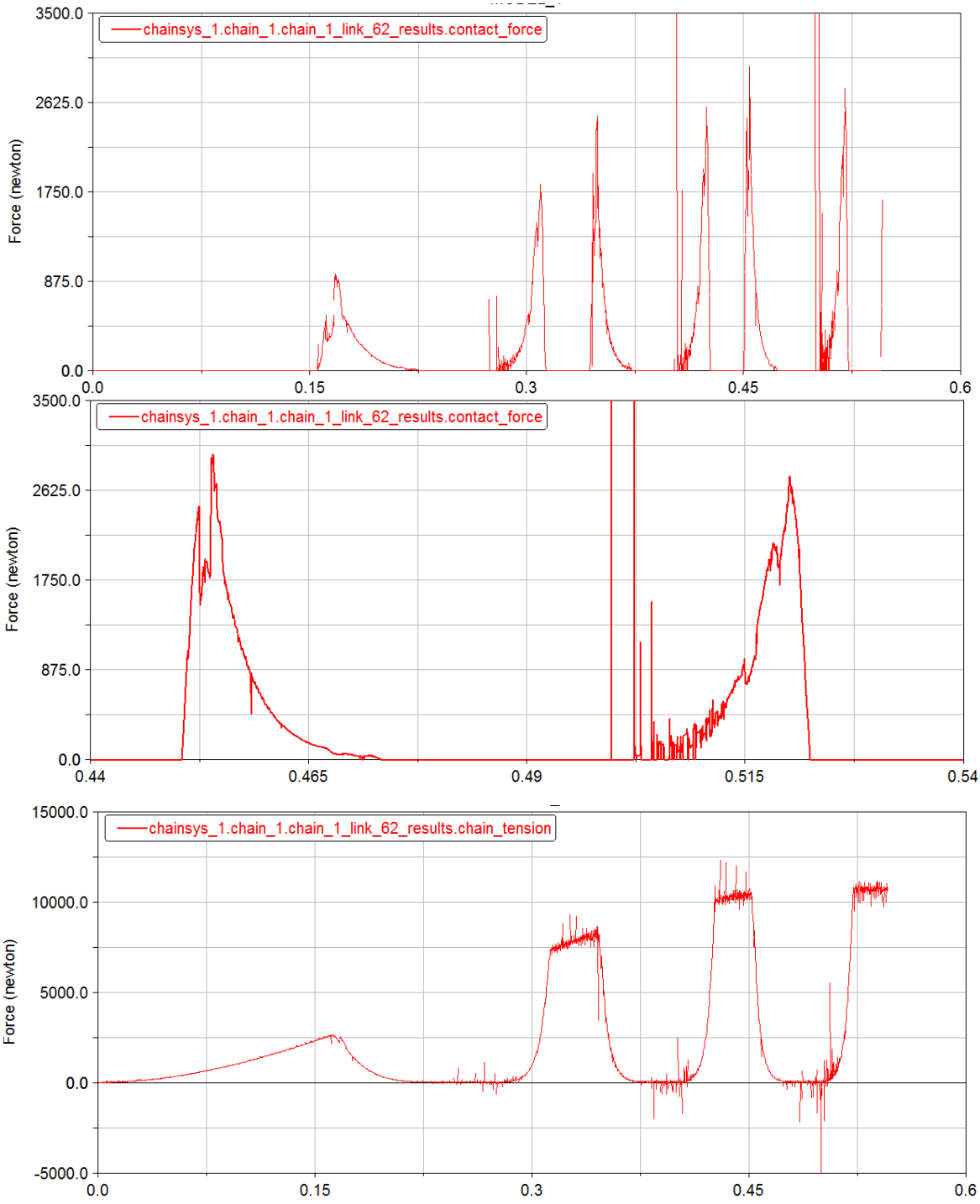

MAX CHAIN TENSION 11300N

MAX CONTACT FORCE 2980N

26.37%

1500 rpm – 500 Nm – 0.2% extension

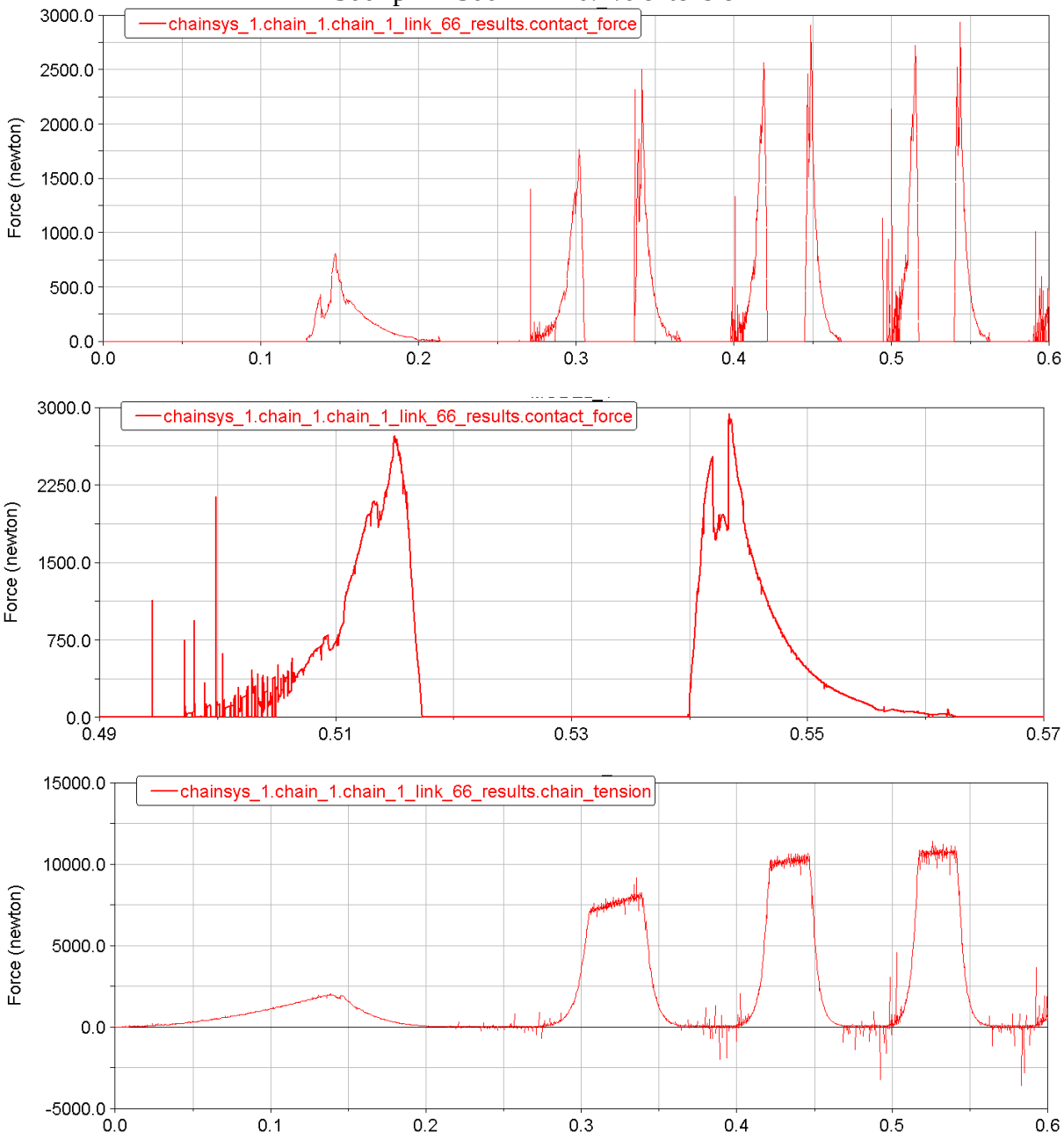

MAX CHAIN TENSION 11110N

MAX CONTACT FORCE 2940N

26.46%

1500 rpm – 1500 Nm – 0.1% extension

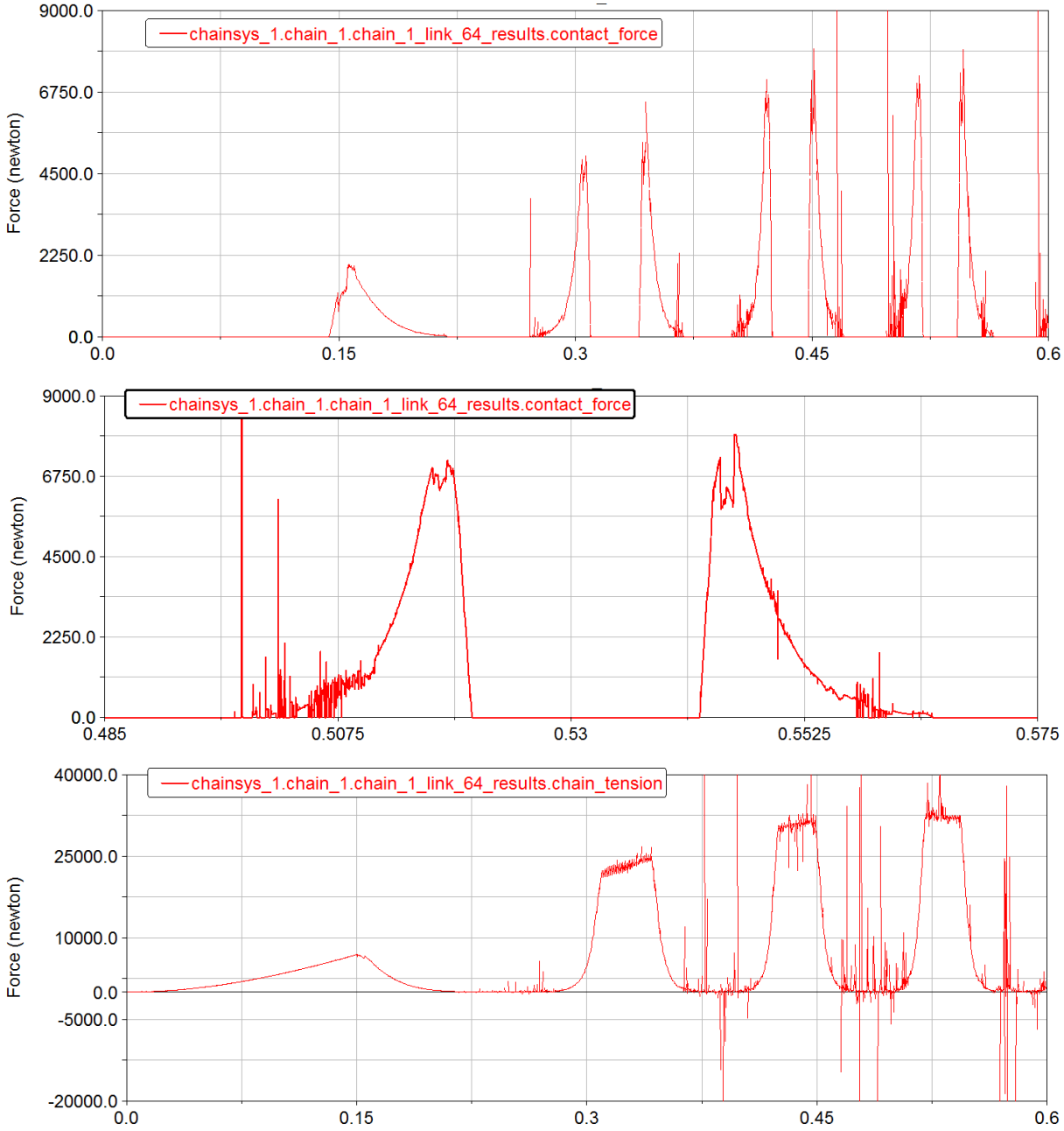

MAX CHAIN TENSION 33070N

MAX CONTACT FORCE 7920N

23.95%

1500 rpm – 1500 Nm – 0.2% extension

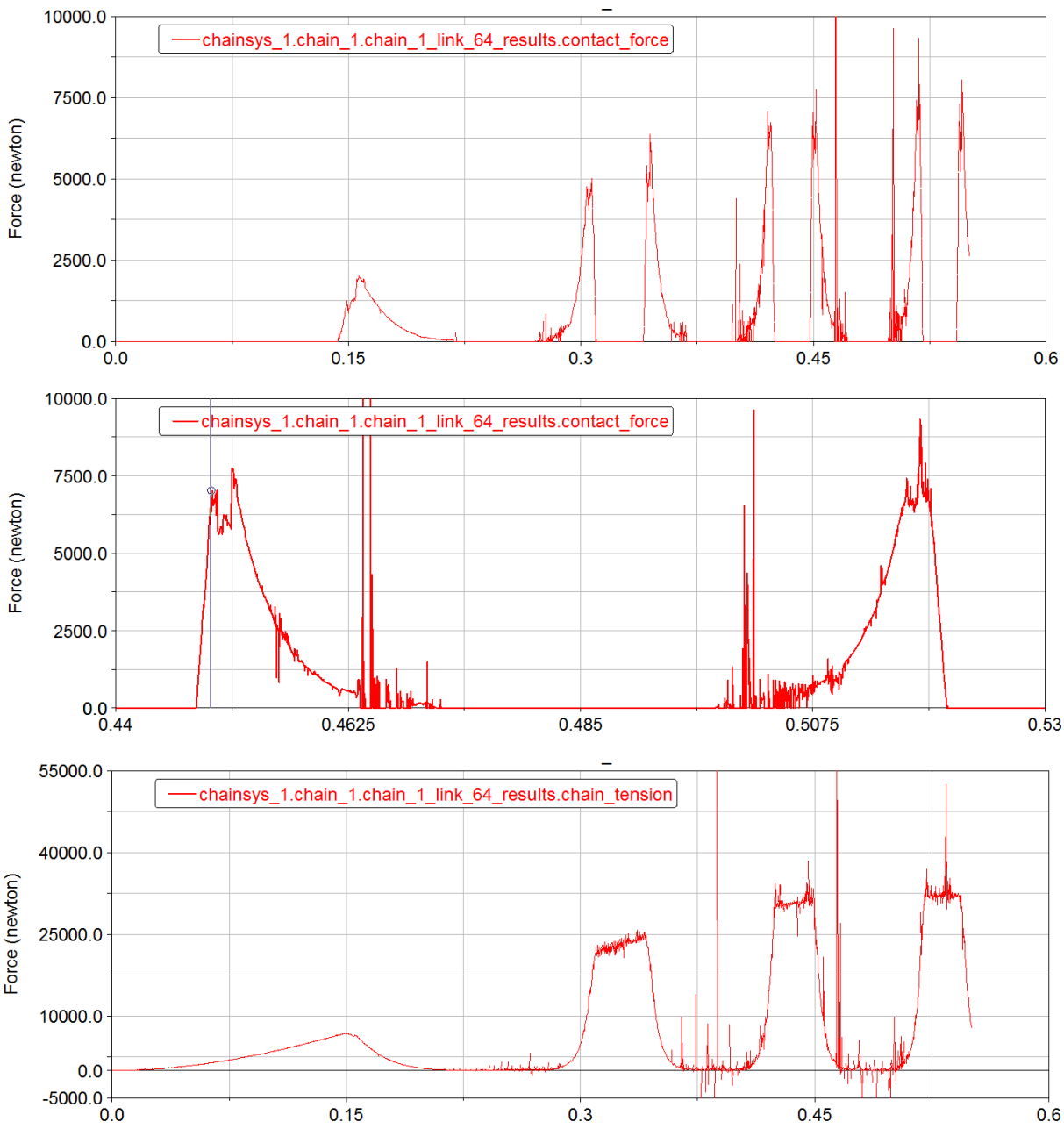

MAX CHAIN TENSION 35200N

MAX CONTACT FORCE 9330N

26.51%